

# **Design and Construction of Experiment for Direct Electron Irradiation of a Uranyl Sulfate Solution: Bubble Formation and Thermal Hydraulics Studies**

---

**Chemical Sciences and Engineering Division**

### **About Argonne National Laboratory**

Argonne is a U.S. Department of Energy laboratory managed by UChicago Argonne, LLC under contract DE-AC02-06CH11357. The Laboratory's main facility is outside Chicago, at 9700 South Cass Avenue, Argonne, Illinois 60439. For information about Argonne and its pioneering science and technology programs, see [www.anl.gov](http://www.anl.gov).

### **DOCUMENT AVAILABILITY**

**Online Access:** U.S. Department of Energy (DOE) reports produced after 1991 and a growing number of pre-1991 documents are available free via DOE's SciTech Connect (<http://www.osti.gov/scitech/>).

### **Reports not in digital format may be purchased by the public from the National Technical Information Service (NTIS):**

U.S. Department of Commerce  
National Technical Information Service  
5301 Shawnee Rd  
Alexandria, VA 22312  
**[www.ntis.gov](http://www.ntis.gov)**  
Phone: (800) 553-NTIS (6847) or (703) 605-6000  
Fax: (703) 605-6900  
Email: **[orders@ntis.gov](mailto:orders@ntis.gov)**

### **Reports not in digital format are available to DOE and DOE contractors from the Office of Scientific and Technical Information (OSTI):**

U.S. Department of Energy  
Office of Scientific and Technical Information  
P.O. Box 62  
Oak Ridge, TN 37831-0062  
**[www.osti.gov](http://www.osti.gov)**  
Phone: (865) 576-8401  
Fax: (865) 576-5728  
Email: **[reports@osti.gov](mailto:reports@osti.gov)**

### **Disclaimer**

This report was prepared as an account of work sponsored by an agency of the United States Government. Neither the United States Government nor any agency thereof, nor UChicago Argonne, LLC, nor any of their employees or officers, makes any warranty, express or implied, or assumes any legal liability or responsibility for the accuracy, completeness, or usefulness of any information, apparatus, product, or process disclosed, or represents that its use would not infringe privately owned rights. Reference herein to any specific commercial product, process, or service by trade name, trademark, manufacturer, or otherwise, does not necessarily constitute or imply its endorsement, recommendation, or favoring by the United States Government or any agency thereof. The views and opinions of document authors expressed herein do not necessarily state or reflect those of the United States Government or any agency thereof, Argonne National Laboratory, or UChicago Argonne, LLC.

# **Design and Construction of Experiment for Direct Electron Irradiation of a Uranyl Sulfate Solution: Bubble Formation and Thermal Hydraulics Studies**

---

by

Sergey Chemerisov, Roman Gromov, Vakho Makarashvili, Thad Heltemes,  
Zaijing Sun, Kent Wardle, James Bailey, Kevin Quigley, Dominique Stepinski,  
and George Vandegrift  
Chemical Sciences and Engineering Division, Argonne National Laboratory

prepared for

U.S. Department of Energy, National Nuclear Security Administration,  
Office of Defense Nuclear Nonproliferation

October 2014



## CONTENTS

ABSTRACT.....	1
1 INTRODUCTION .....	2
2 DESIGN OF THE EXPERIMENTAL APPARATUS .....	4
3 COMPUTATIONAL FLUID DYNAMICS SIMULATIONS.....	9
3.1 Multiphase CFD Simulations using OpenFOAM.....	9
3.2 Simulation Using ANSY CFX.....	11
4 ENGINEERING DESIGN ANALYSES .....	14
4.1 Structural Analysis of the Electron-Beam Raster Vacuum Chamber .....	14
4.2 Structural Analysis of the Inner Chamber .....	16
4.3 Thermal-Hydraulic Analysis of the Cooling System for the Bubble Chamber .....	17
5 MONTE CARLO SIMULATIONS .....	21
5.1 Power Deposition Distributions.....	22
5.2 Activation Study .....	23
5.3 Post-irradiation Exposure Rates.....	25
6 PREPARATION OF THE 20-L URANYL SULFATE SOLUTION .....	28
7 CONCLUSIONS .....	29
8 REFERENCES .....	30
9 ACKNOWLEDGEMENT .....	31
APPENDIX A: Bubble Chamber Assembly Status Photographs: 9-22-2014 .....	33
APPENDIX B: Mechanical Spec Sheets and Modelling.....	51

## FIGURES

1 Layout of the Experimental Setup .....	5
2 A Detailed View of the Solution Chamber .....	6

## FIGURES (Cont.)

3	Annotated Schematic of the Bubble-Chamber Assembly .....	7
4	Maximum and Average Temperature of the Solution with and without Bubbles Present.....	10
5	Plots of Temperature Profile and Velocity Fields at the Last Time Step Simulated for 2-D Simulations Using Laminar Flow Assumption with and without Gas Introduction and LES Turbulence.....	11
6	Plots of Instantaneous and Time-Averaged Temperature and Velocity Vector Fields from 3-D Simulations.....	12
7	Temperature and Velocity Profiles for 20 L Solution Volume.....	13
8	Design of the Stress-Analysis Vacuum Raster Chamber.....	14
9	Calculated Von Mises Stresses on Vacuum Raster Chamber.....	15
10	Calculated Deflections in the Vacuum Raster Chamber.....	15
11	Weld Analysis .....	16
12	P/I Diagram for the Bubble Chamber Cooling System .....	18
13	FATHOM Computer Model for Bubble-Chamber Cooling System .....	19
14	MCNPX Geometry Model for Bubble Formation Experiment .....	21
15	Spatial Profile of the Electron Beam Used in MCNPX Simulations.....	22
16	Fractional Power Deposition in Each Cell.....	23
17	Photon Flux Distribution per Kilowatt of Beam Power.....	24
18	Activity Levels of Major Activation Products in the Sodium Sulfate Solution .....	25
19	Total Activities for Each Cell Versus Decay Time .....	26
20	Total Activity of the Uranyl Sulfate Target with and Without Photo-Fission.....	26
21	Exposure Rate Results at 30 cm for All Four Cases .....	27

## TABLE

1	Camera Information .....	5
---	--------------------------	---

*This page intentionally left blank*



# **DESIGN AND CONSTRUCTION OF EXPERIMENT FOR DIRECT ELECTRON IRRADIATION OF A URANYL SULFATE SOLUTION: BUBBLE FORMATION AND THERMAL HYDRAULICS STUDIES**

## **ABSTRACT**

Argonne is assisting SHINE Medical Technologies in developing SHINE, a system for producing fission-product  $^{99}\text{Mo}$  using a D/T-accelerator to produce fission in a non-critical target solution of aqueous uranyl sulfate. We have developed an experimental setup for studying thermal-hydraulics and bubble formation in the uranyl sulfate solution to simulate conditions expected in the SHINE target solution during irradiation. A direct electron beam from the linac accelerator will be used to irradiate a 20 L solution (sector of the solution vessel). Because the solution will undergo radiolytic decomposition, we will be able to study bubble formation and dynamics and effects of convection and temperature on bubble behavior. These experiments will serve as a verification/ validation tool for the thermal-hydraulic model. Utilization of the direct electron beam for irradiation allows homogeneous heating of a large solution volume and simplifies observation of the bubble dynamics simultaneously with thermal-hydraulic data collection, which will complement data collected during operation of the mini-SHINE experiment. Irradiation will be conducted using a 30-40 MeV electron beam from the high-power linac accelerator. The total electron-beam power will be 20 kW, which will yield a power density on the order of 1 kW/L. The solution volume will be cooled on the front and back surfaces and central tube to mimic the geometry of the proposed SHINE solution vessel. Also, multiple thermocouples will be inserted into the solution vessel to map thermal profiles. The experimental design is now complete, and installation and testing are in progress.

## 1 INTRODUCTION

SHINE Medical Technologies is planning to use neutron-induced fission in a subcritical liquid target for production of  $^{99}\text{Mo}$ . During operation, the solution will undergo radiolytic decomposition. Because formation of the bubbles and their size and dynamics will impact operational parameters of the liquid target, an understanding of bubble behavior is critical for the ability to predict the behavior of the salt solution during operation. In this proposed experiment, we will be using the electron beam of a linear accelerator to irradiate a solution volume (sector of the solution vessel) to study the thermal hydraulics of the system. Experimental results obtained in this task will be compared with simulations to fine tune computer models. Because the solution will undergo radiolytic decomposition from electrons slowing down in the liquid, we will be able to study bubble formation and dynamics and effects of convection and temperature on bubble behavior. These experiments will serve as a verification/validation tool for the thermal-hydraulic model. While data on radiolytic gas formation will be collected in mini-SHINE experiments, data for bubble-formation dynamics in these experiments will be limited due to the complexity of the optical setup for the extremely high radiation fields in the fissioning solution. Utilization of the direct electron beam irradiation allows homogeneous heating of a large solution volume and simplifies simultaneous observation of the bubble dynamics with thermal-hydraulic data collection.

Irradiation will be conducted by using a 30-40 MeV electron beam from the high-power linear accelerator. This range of electron-beam energy translates into 13-17 cm of an average range of electrons in water, so we can use a large solution volume to study convective behavior resembling the bulk solution. The electron beam can be raster scanned and focused in such a way that the whole volume of the 15-cm x 15-cm x 80-cm solution is homogeneously heated. The total electron-beam power will be 20 kW, which will yield a power density on the order of 1 kW/L. This power can be uniformly distributed in the solution due to the low linear energy transfer (LET) of the high energy electrons. The beam-scan frequency will be high enough (up to 240 Hz) to ensure uniform power distribution within the convection time constant of the solution.

The solution volume will be actively cooled on the front and back surfaces and central tube to mimic the geometry of the proposed SHINE solution vessel. Sides of the irradiation volume will be constructed from optical quartz, so bubble formation and propagation can be observed by means of cameras. Also, multiple thermocouples will be inserted into the solution to map its thermal profiles.

According to literature data, gas generation due to electron radiolysis is expected to be one-fourth that due to fission fragments, but we can vary the power density in the solution to make up for the difference in generation rate. We will combine bubble dynamic observation with gas-generation measurements using a residual gas analyzer (RGA) to establish a correlation between bubble dynamics and time required for establishing the steady-state concentrations and onset of oxygen formation. We will irradiate water as well as a uranium salt solution to study the thermal hydraulics of the system.

Before final design of the bubble experiment, preliminary testing of concepts and equipment was performed in a series of experiments at the Van de Graaff (VDG) generator. These studies can be found in a separate report [1].

## 2 DESIGN OF THE EXPERIMENTAL APPARATUS

The experimental setup for direct electron irradiation consists of the beam line and beam optics, a water-cooled solution chamber, a camera for bubble detection, and a cooling system. A schematic of the experimental setup is shown in Figure 1. The beam optics consists of a pair of quad magnets and pair of dipole magnets. This arrangement allows us to distribute the electron beam over the whole solution volume. The quad-magnet pair is used to control the dimensions of the electron beam at the target, while the dipole pair is used to scan the beam in the vertical and horizontal directions.

A primary goal of this experiment is to determine the size, hold-up, and, if possible, the velocity of gas bubbles generated by radiolytic production of hydrogen and oxygen in the solution under irradiation. From preliminary experiments under electron irradiation at the VDG facility, it is expected that the bubble size may be as small as 100  $\mu\text{m}$ . As such, careful consideration of camera, lensing, and lighting is required to obtain useful images of such small features. Additional challenges are posed by the radiation field of the system, which requires a standoff distance of 1.5 m. Given these challenges, perhaps the most critical piece of equipment is the lens. A K1 CentriMax long-range microscope lens system from Infinity USA will be used. This lens has configurable objectives lenses, including a long range (LR) option to allow for small feature imaging at standoff distances up to 3 m, along with capability for remote focusing. Two cameras will be used for imaging of the experiment: a CAM1 having higher frame-rate capability for use with the K1 CentriMax lens for capturing bubble size/motion, and a CAM2 having higher resolution (and lower frame rate) for capturing a wider view of the experiment (see Table 1 for camera details). Both cameras use a USB 3.0 connection, which is essential for the high data transfer rates required. CAM1 when used in conjunction with the K1 CentriMax lens will have a field of view of less than 1 cm  $\times$  1 cm and will be mounted on a custom X/Y traverse system (controlled by a LabView interface) capable of moving the camera to any point of the viewing window. The traverse system and both cameras are mounted on a custom table with a 3-ft-high wall of lead bricks 4-in. thick to provide adequate shielding. The cameras will be oriented parallel to the beam (with the lead wall in between) with a 12-in.  $\times$  36-in. first surface mirror positioned in front of the camera and oriented at 45 degrees to allow for a view of the chamber and imaging window.

Lighting will be provided from the back side of the chamber through a second set of windows opposite those from the camera side. Backlighting is ideal for good contrast in multiphase systems such as this. Even so, the small field of view, large stand-off distance, and high frame rate (short exposure time) required by the measurements present a challenge for providing adequate lighting. Additionally, the lights also must be shielded, positioned at stand-off distance of  $\sim 2$  m, and redirected by mirrors to the lighting window. Given these challenges, a somewhat unorthodox solution had to be considered for lighting. It is planned to use three high-power (250 W) LED stage spotlights (Altman Phoenix Profile Spotlight, Model PHX-5600K-10-B) oriented in a vertical stack. Preliminary experiments at the VDG using the same lens system at a 5-ft standoff showed that adequate lighting could be provided by three in-house constructed 100 W LED lights at close range. It is anticipated that the selected configuration (a total of 750 W of LED lighting) should provide sufficient lighting for the

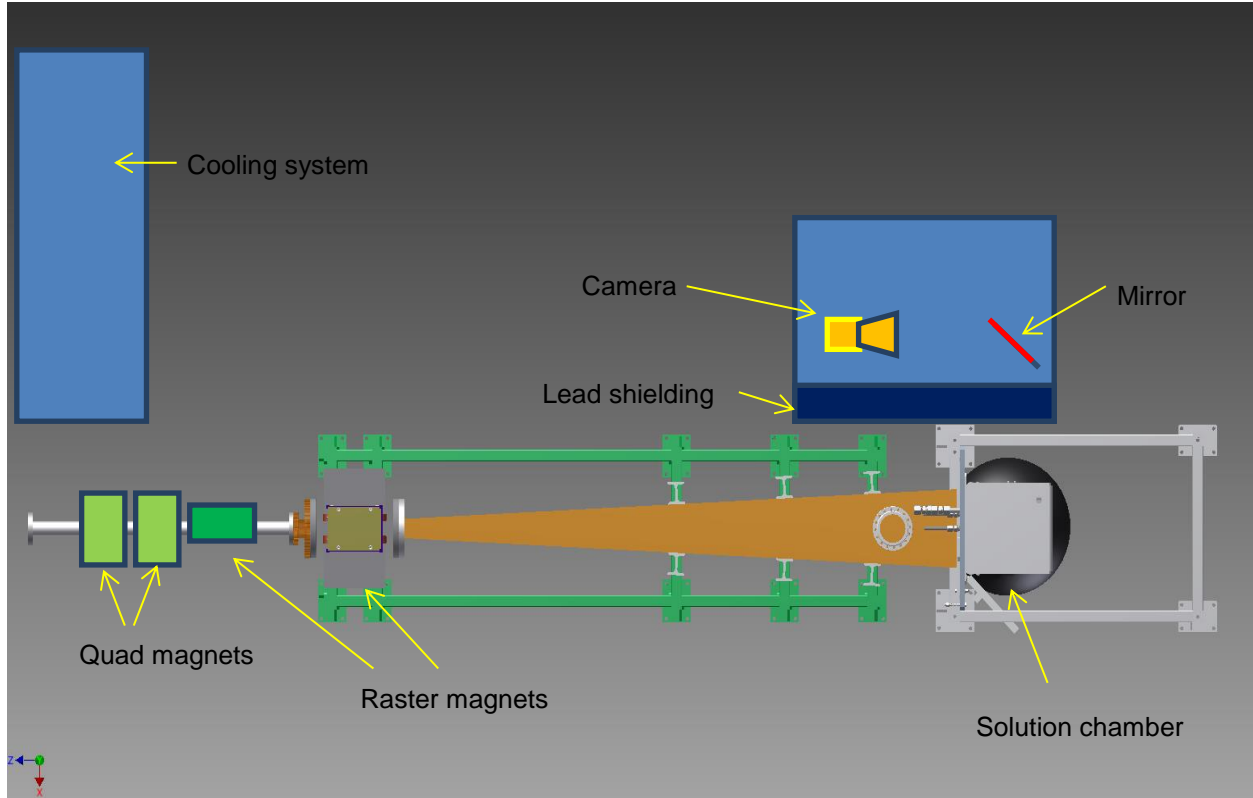


**FIGURE 1 Layout of the Experimental Setup**

**TABLE 1 Camera Information**

Camera	Model	Frame Rate @ Resolution
CAM1	PointGrey Grasshopper3, Model GS3-U3-23S6M-C	160 frames/second @ 2.3 MP (mono)
CAM2	PointGrey Flea3, Model FL3-U3-88S2C-C	21 frames/second @ 8.8 MP (color)

intended measurements. Performance of the imaging and lighting systems will need to be confirmed during cold tests of the bubble chamber experiment. Because of the high radiation field near the solution volume, we have to use a mirror, so that the camera is not in the line of site of the bremsstrahlung photons generated in the target housing and solution. Our calculations showed that six inches of lead will be sufficient to shield the camera.

Details of the chamber assembly are shown in Figures 2 and 3. The assembly contains a rectangular sealed vessel that contains the uranyl sulfate solution. The electron beam enters the vessel through a beam window located at the left-side wall. The outer surface of this wall

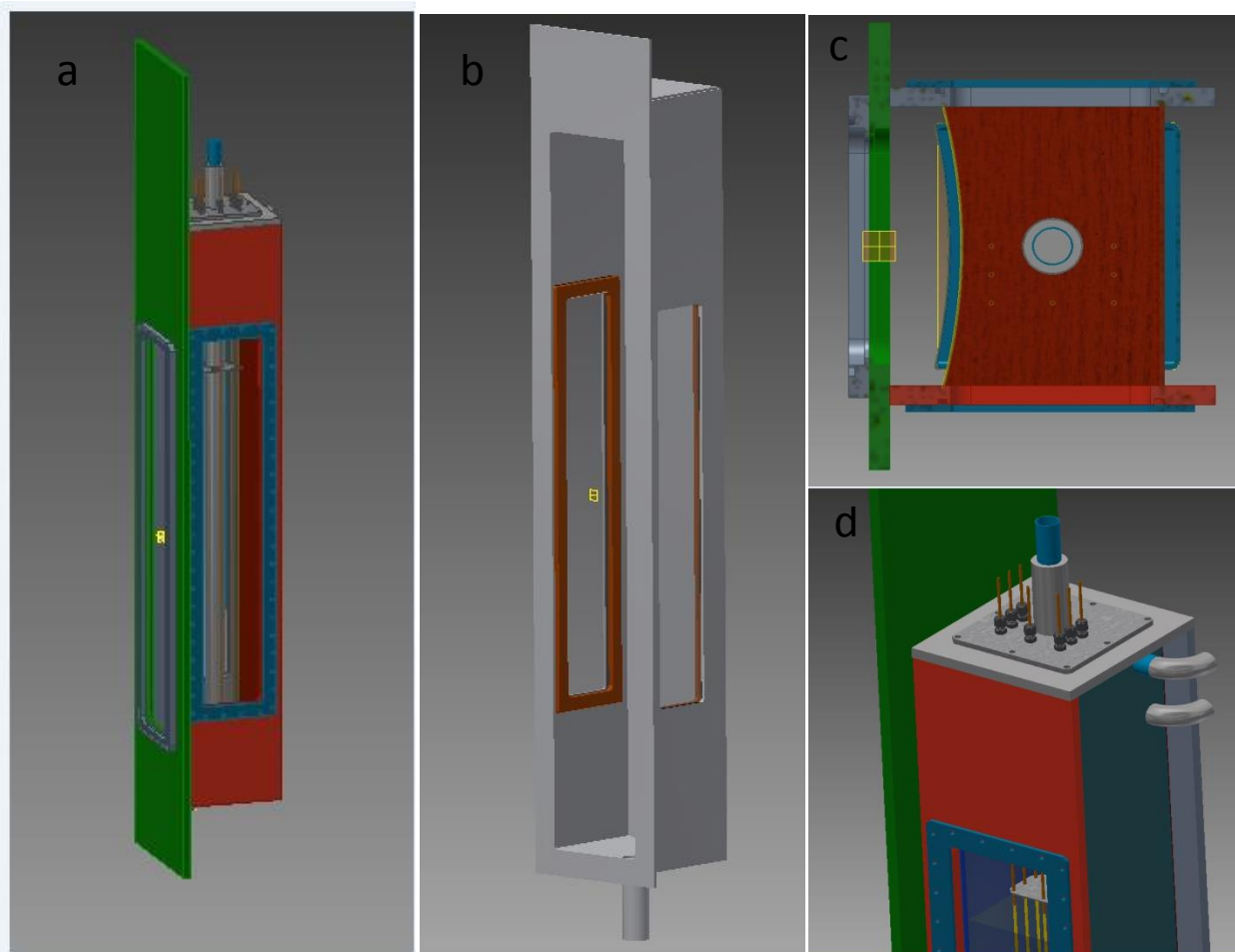


**FIGURE 2 A Detailed View of the Solution Chamber: a. Main solution chamber. b. Secondary aluminum enclosure. c. Top view of the main solution chamber. d. Close-up view of the top portion of the main solution chamber showing position of the central cooling tube and penetrations for thermocouple assemblies.**

interfaces with the raster vacuum chamber in the beam line. There is an O-ring seal at this interface. The beam window is double walled to allow for coolant flow between the walls. Also, the thickness of these walls has been minimized to reduce the loss of the beam in the wall material. The two side walls have quartz windows for visual inspection of the solution during irradiation. The right side wall as well as the bottom wall is doubled-walled to also provide for coolant flow. In addition, there is a drain and fill tube connection in the bottom wall of the vessel. The vessel's top plate contains penetrations for thermocouple assemblies, a coolant center tube, and additional penetrations for venting and purging. The chamber is a welded all-stainless-steel construction. The pressure in the vessel will be kept sub-atmospheric. Sweep gas (helium) will be introduced into the head space of the chamber. The flow rate of the cover gas will be adjustable so the concentration of the radiolytically produced hydrogen will be maintained below one percent. The sweep gas will be collected in the gas collection system of the mini-SHINE experiment. The composition of the gas will be continually monitored by a gas monitoring system. This arrangement will allow us to measure radiolytic gas generation rates.

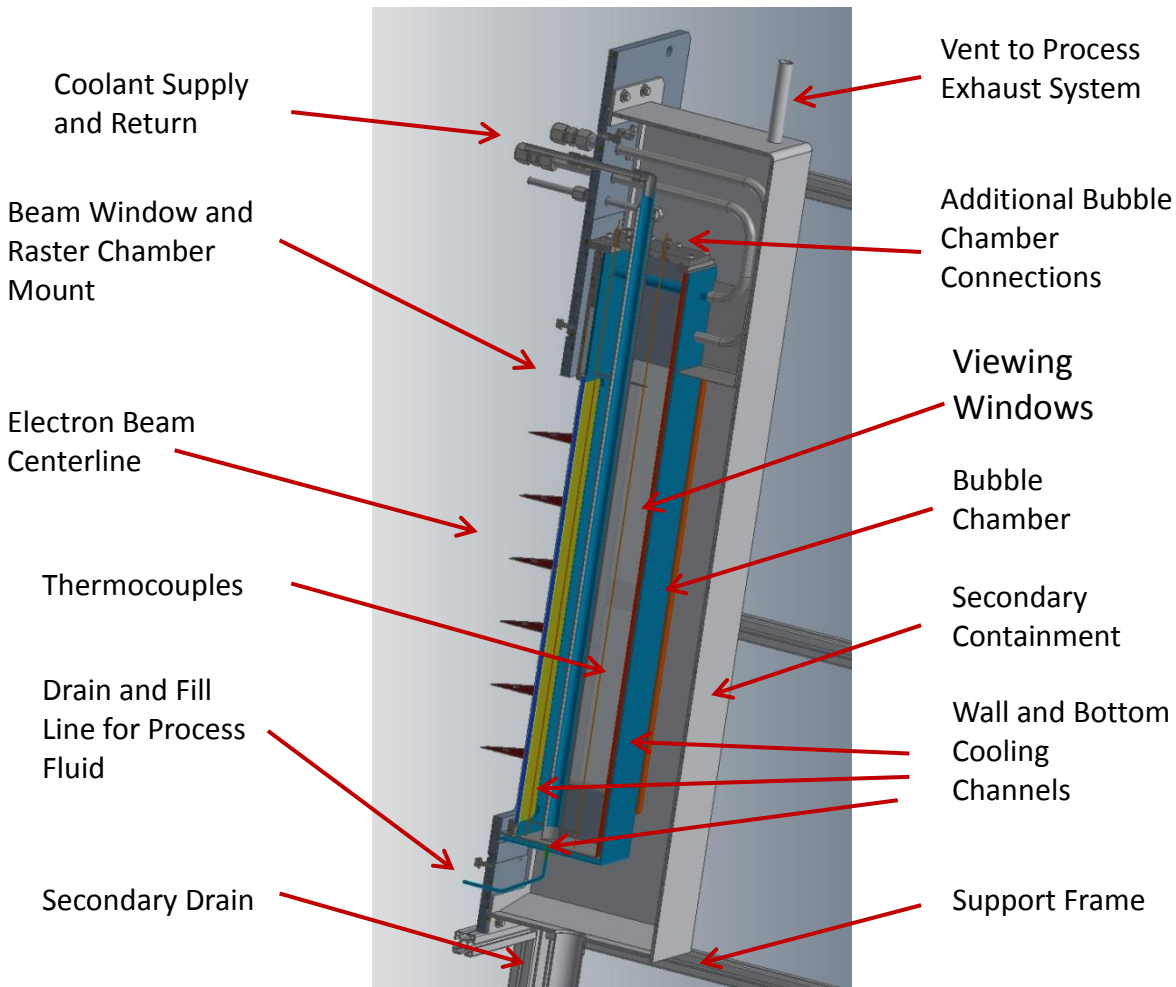


**FIGURE 3 Annotated Schematic of the Bubble-Chamber Assembly**

The solution chamber is equipped with seven thermocouple assemblies, each having six measuring points, so we will be able to measure the temperature of the solution in 42 points simultaneously.

A secondary chamber (Figure 2b) is installed around the solution chamber to mitigate a containment failure of the primary vessel. The left side wall of the secondary chamber interfaces with the inside surface of the primary left-side (beam side) plate and is sealed with an O-ring. The side walls have quartz windows to allow observation of the bubbles in the solution. These windows are aligned with the primary windows. A 2-in. drain is located in the bottom of the chamber and is connected to an external holding tank. The secondary containment is not intended to hold the entire inventory of the process fluid. Therefore, any leakage into the secondary chamber must be free to drain to the holding tank. Also, there is a vent in the top plate of the secondary chamber that is connected to the process exhaust system, causing the secondary chamber to have a slightly negative pressure relative to the room pressure. The secondary chamber is a welded aluminum construction.

The cooling system for the experiment is designed to have sufficient capacity to remove 20 kW of heat. A cooling-water pump is sized to provide 50 gpm of water flow at up to 50 psig pressure. The cooling system has an all-welded design. All components are stainless steel and equipped with a mixed-bed deionizer to remove possible contaminants from the cooling water. The head space of the make-up tank is purged by air and is vented through the HEPA-filter equipped exhaust system to prevent hydrogen buildup. All elements of the cooling system that are not welded are located inside an enclosure to prevent spread of suspect coolant water to the environment. This enclosure is also connected to the exhaust system.

As of September 25, 2014, the apparatus is still under construction. Appendix A is a pictorial record of the components as of September 22<sup>nd</sup>. The main chamber is constructed, has been leak-tested with helium gas, and is currently filled with water as a final leak test. The secondary chamber will now be assembled around the primary, and the cameras will be mounted. Experiments should begin in the first half of October.



### 3 COMPUTATIONAL FLUID DYNAMICS SIMULATIONS

Two engineers have used different computational fluid dynamics (CFD) simulation packages to calculate the temperature in the irradiated solution—OpenFOAM and ANSYS CFX. The two computer models yield quite different results; ultimately, experimental measurements will provide information to verify the computer model. For the actual experiment, power will be brought up slowly to avoid the overheating that one of the models predicts. These two CFD methods are discussed below.

#### 3.1 MULTIPHASE CFD SIMULATIONS USING OPENFOAM

Preliminary multiphase CFD simulations were conducted using a custom solver built in the OpenFOAM toolkit (version 2.1.x) and based on the Eulerian-Eulerian multi-fluid methodology with additional capability for sharp interface capturing (*multiphaseEulerFoam* solver) [2]. Solution of the energy transport equation along with density variations using the Boussinesq approximation were also incorporated into the solver. We performed 2-D and 3-D simulations for a box with dimensions of 15 cm  $\times$  15 cm  $\times$  1 m (with 80 cm of liquid and a 20 cm headspace). The 2-D case used for initial scoping included 16,700 hex cells. The 3-D model consists of a total of  $\sim$ 900K hexahedral cells with a base mesh size of 3 mm and additional refinement in the wall layer with a minimum thickness in the wall normal direction of  $\sim$ 1 mm. We performed simulations using a uniform volumetric heat generation rate of 20 kW as well as a block-averaged profile (in the beam penetration direction) taken from Monte Carlo particle transport code calculations (MCNPX). The total generation rate was 15 kW. Wall temperature was held at 20°C. For this set of simulations, rather than as a volumetric source proportional to the volumetric heat generation, the introduction of the radiolytically produced gas was from the inner wall with a flow rate equivalent to a volume fraction of 1% (1.5 mL/s). A bubble size of 1 mm was assumed, and a virtual mass coefficient of 0.5 was used. The properties of the gas phase were taken as the stoichiometric average of hydrogen and oxygen. The influence of the introduction surface for gas bubbles (bottom versus side) was explored and found to have minimal influence. As the flow in these conditions is expected to be in the turbulence transition regime, the role of turbulence modeling was also expected to be important and was explored with the use of the laminar flow assumption and the fully-transient large eddy simulation (LES) (using the Smagorinsky sub-grid model [3]).

We found that the negative impact of the thermal conductivity of the gas phase had a significant influence on the overall temperature profiles, much more than the convective flow magnitudes (and correspondingly the assumed droplet size). Figure 4 shows a plot of the average and maximum temperatures as a function of time from startup for the 2-D simulations (laminar) with and without gas bubbles in the liquid.

When the upper free surface of the liquid was included in the model, motion of the liquid surface was not substantial; however, currents in the gas headspace, which develop much more quickly than in the liquid, did have an important influence on the initial development of the natural convection loop in the upper section of the liquid volume. The role of turbulence was

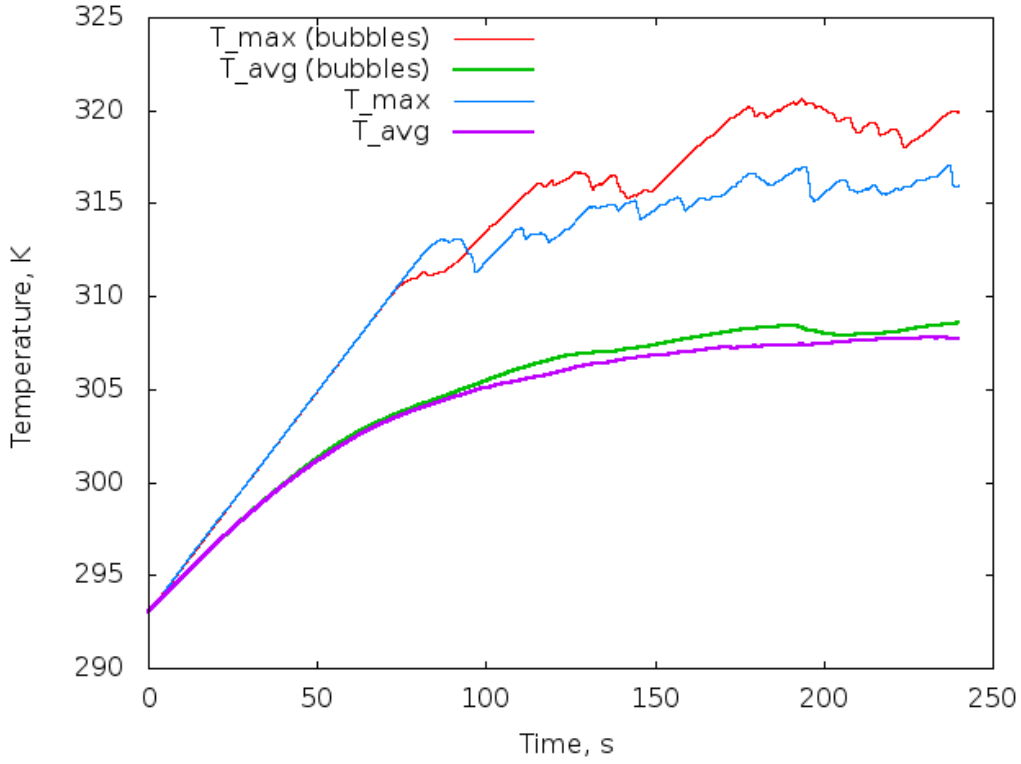


**FIGURE 4 Maximum and Average Temperature of the Solution with and without Bubbles Present**

also critically important to the overall heating; the maximum temperature of the fluid volume was found to increase much more significantly when laminar flow is assumed as compared to large-eddy simulation (LES) of turbulence. Figure 5 shows contour plots of temperature and velocity vectors for the different turbulence treatment as well as for cases with and without gas introduction. In the absence of the additional driving force of the buoyant flow of the gas bubbles, we observed that the natural circulation loop in the gas headspace had a significant influence on the flow pattern of the liquid phase. Additional radial momentum was transferred to the upper region via the liquid free surface and multiple counter-rotating “cells” were formed rather than a vertically continuous loop, as might otherwise be expected and is seen in the case with gas bubble introduction; however, this phenomena appeared to be much more pronounced in 2-D simulations.

Using LES and 3-D simulations incorporating additional boundary layer refinement along the vertical walls, we found the overall temperature rise to be less than 20°C. A comparison of instantaneous and time-averaged temperature and velocity fields is given in Figure 6. A transient downward flow pattern was observed near the vertical walls with the flow shedding radial vortices while traveling downward. However, when observed as a time-averaged values, the general path of the flow can be seen as a pseudo-steady upward plume with downward flow at the walls. The maximum rise velocity of the “plume” did not exceed a few centimeters per second, and the downward flow at the walls approached 4~5 cm/s. The details of the treatment of wall boundaries with regard to heat transfer in the boundary layer were also found to be of

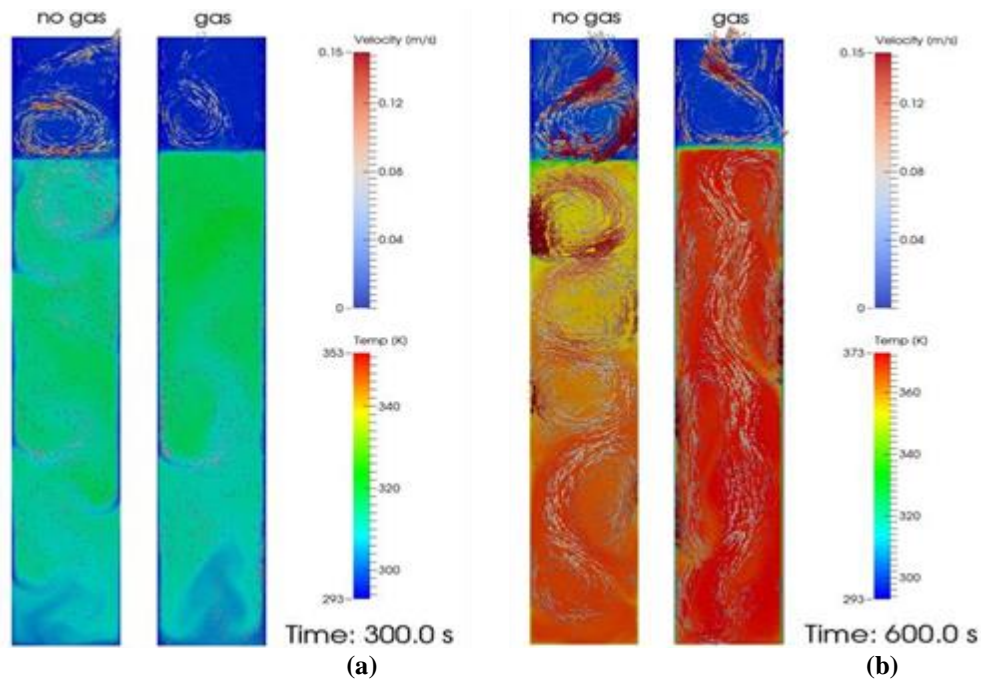


**FIGURE 5 Plots of Temperature Profile and Velocity Fields at the Last Time Step Simulated for 2-D Simulations Using (a) Laminar Flow Assumption with and without Gas Introduction and (b) LES Turbulence. The beam (and gas introduction) is from the left.**

importance to the overall heat transfer observed. In this case, the effective increase in thermal diffusivity in the boundary layer due to turbulence was accounted for by using a turbulent Prandtl number of 0.9.

### 3.2 SIMULATION USING ANSYS CFX

We have also performed hydraulic analysis of the process fluid under irradiation using the ANSYS CFX computer code. For these simulations, we assumed a rectangular fluid volume with a 10 kW uniform heat generation due to beam heating. The boundaries at the left, right, and bottom walls (walls that are cooled by forced convection) were assumed to be at a constant temperature near ambient (i.e., coolant temperature). The two side walls (walls with no cooling and with viewing windows) were assumed to be insulated. Also, the free surface at the top of the process fluid was assumed to be insulated, and cooling by evaporation of water was not taken into account. The process fluid properties were assumed to be that of water.

The temperature and velocity profiles through the center of the chamber are shown on Figure 7. The maximum temperature in the fluid is 81°C at the 10-kW heat generation rate. Essentially, the analysis indicates that a heat generation significantly above the 10 kW would result in boiling in the fluid. The velocity profile shows the weak natural convection flow within the fluid. The resulting high thermal convective resistance inherently limits the maximum beam power for irradiation of the fluid.

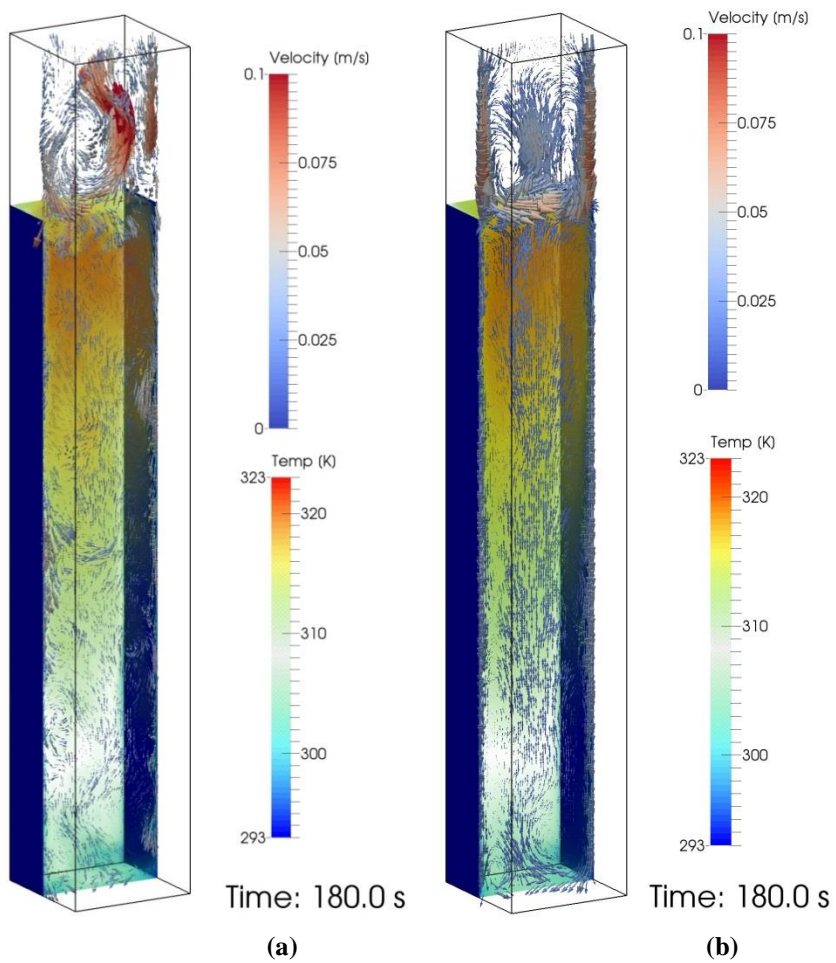


**FIGURE 6 Plots of (a) Instantaneous and (b) Time-Averaged Temperature and Velocity Vector Fields from 3-D Simulations**

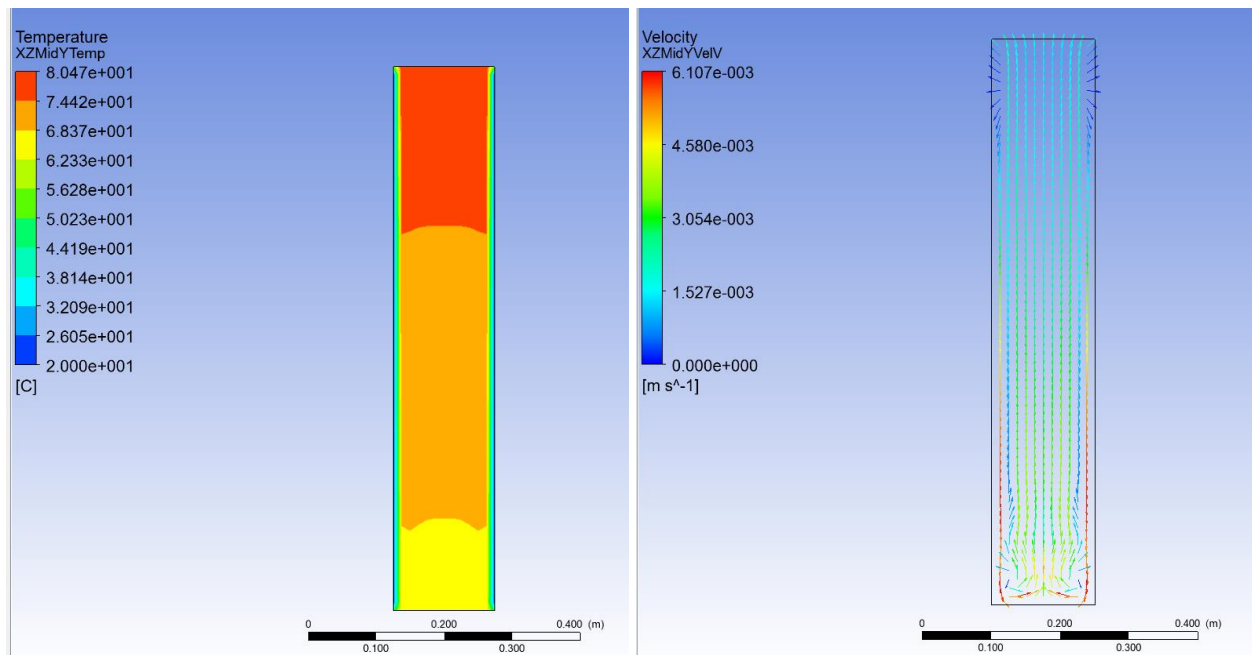


**FIGURE 7 Temperature and Velocity Profiles for 20 L Solution Volume. Power deposition in solution is 10 kW.**

## 4 ENGINEERING DESIGN ANALYSES

Presented below were analyses performed on two key engineering designs in the experimental apparatus.

### 4.1 STRUCTURAL ANALYSIS OF THE ELECTRON-BEAM RASTER VACUUM CHAMBER

We performed a structural analysis of the electron-beam raster vacuum chamber using ANSYS Mechanical 15.0 software. The analysis utilized quarter symmetry and assumed 1 atm of external pressure. The initial design of the chamber incorporated 3/8-in.-thick 6061 aluminum walls. Initial analysis of the vacuum chamber indicated that additional structural elements were necessary to reduce both mechanical stress and distortion from external pressure. Additional stiffness was provided by inclusion of six I-beams that have a depth of 3 in. and a flange width of 2.5 in. The chamber is depicted in Figure 8.

The stress and deflection plots for the chamber are shown on Figures 9 and 10, respectively. The maximum stress in the chamber is 17.3 kpsi at the end of a tee where the top wall meets the side wall. The maximum deflection occurs in the side wall with a value of 2.4 mm. The final results led to a design with 3/8-in.-thick plates plus six additional I-beam elements to reduce stress and deflection to 10,000 psi and 1.4 mm, respectively.

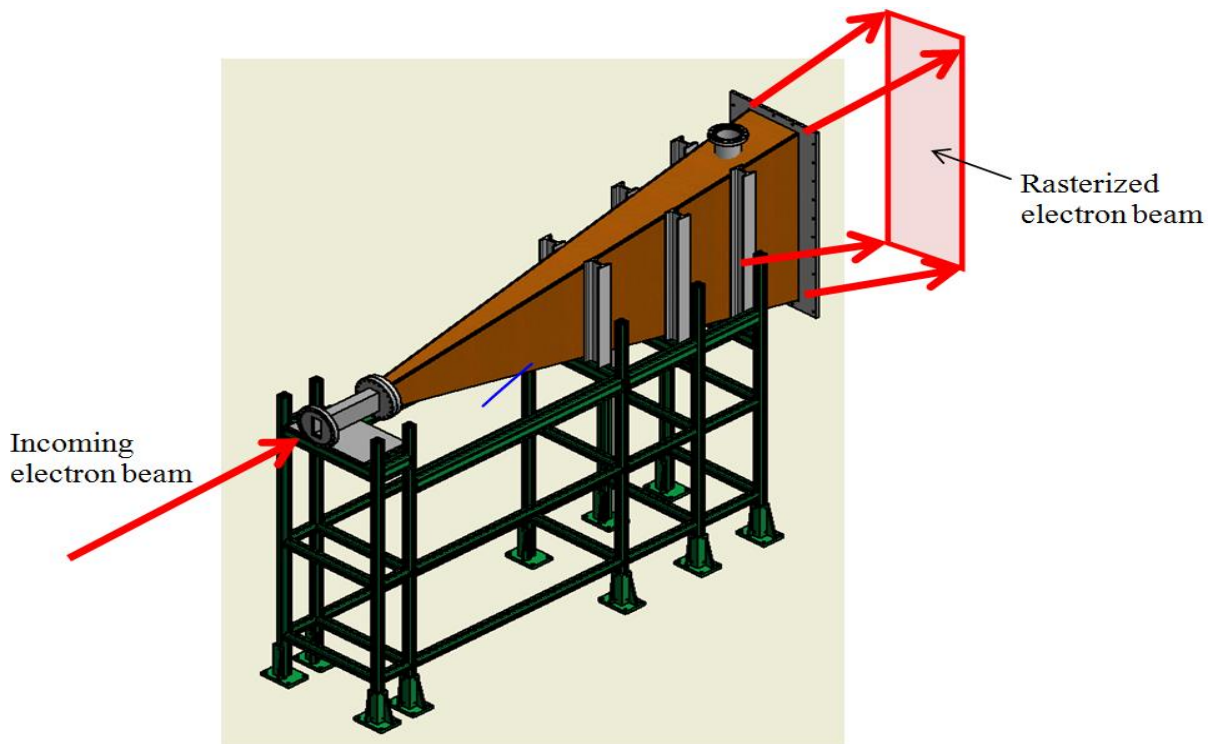


**FIGURE 8** Design of the Stress-Analysis Vacuum Raster Chamber

**D: Copy of aluminum**  
 Equivalent Stress  
 Type: Equivalent (von-Mises) Stress - Top/Bottom  
 Unit: psi  
 Time: 1  
 Custom  
 Max: 9954.7  
 Min: 0.84904

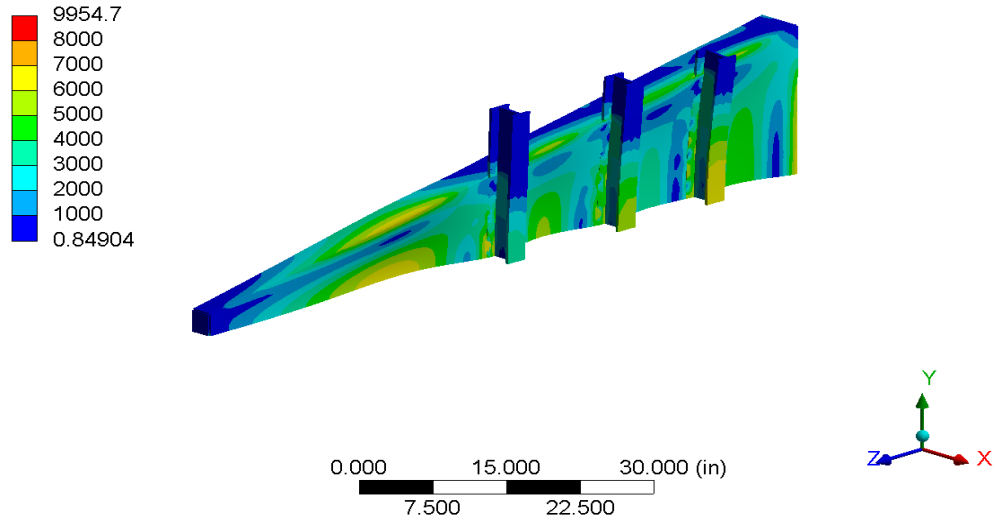


**FIGURE 9 Calculated Von Mises Stresses on Vacuum Raster Chamber**

**D: Copy of aluminum**  
 Total Deformation  
 Type: Total Deformation  
 Unit: mm  
 Time: 1  
 Custom  
 Max: 1.6064  
 Min: 6.0324e-5

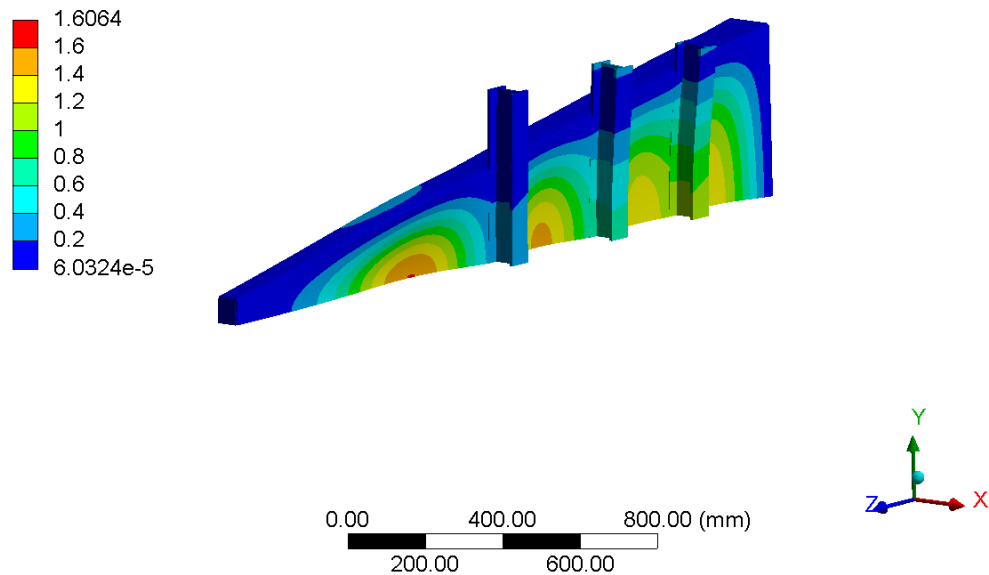


**FIGURE 10 Calculated Deflections in the Vacuum Raster Chamber**

A weld analysis was also performed, and the results appear in Figure 11.

An American Society of Mechanical Engineers (ASME) design stress analysis found a safety factor of 2, and a fillet welds filler analysis found a safety factor of 1.6 for the filler-metal yields. This chamber is not a “pressure vessel” according to the criteria defined in the Argonne *Pressure Systems Safety Manual*. Using a static structural analysis, we determined that the chamber walls do not exceed allowable design stresses listed in the stress tables for 6061-T6 aluminum in the ASME *Boiler and Pressure Vessel Code*.

## 4.2 STRUCTURAL ANALYSIS OF THE INNER CHAMBER

The large size of the water-cooled beam window and our desire to minimize material thicknesses, which cause beam losses, represented a significant engineering challenge. The solution we found included a curved window to resist buckling. Static structural analysis of the beam window separating the electron beam and the process fluid was performed with the ANSYS computer model. The window uses a double-wall design to allow coolant flow. The window design employs a 15-in. cylindrical radius to maintain the necessary rigidity while minimizing material thickness. The side toward the vacuum chamber must resist a pressure differential of 24.7 psi.

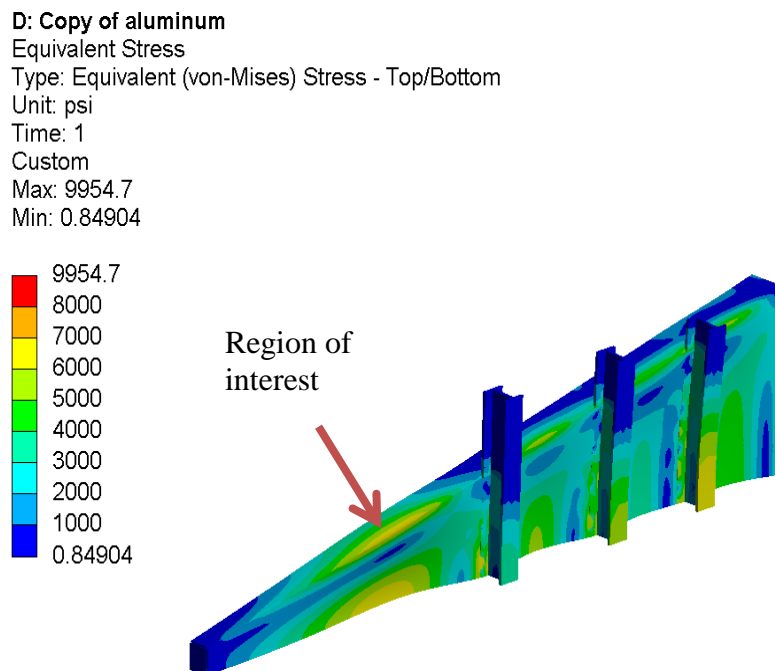


**FIGURE 11 Weld Analysis.** The welded region subjected to higher stress is indicated by the arrow. Stress in the weld is below 60% of the filler metal yield strength (19 ksi).



Initial results from the analysis showed that the main concern in the window design is the ability to provide sufficient rigidity to resist buckling. A linear buckling analysis was performed, based on the static structural analysis, and the design was adjusted to withstand buckling from a differential pressure of 50 psi. However, during leak testing of the window assembly, we observed a tendency to buckle, which was probably due to deformation of the windows during fabrication. This condition necessitated supplemental stiffening with six ribs. The real curvature of the window was measured, and each rib was cut to precisely reflect this curvature. Those ribs were welded to the vacuum side of the window assembly. Consecutive testing of the window assembly showed no buckling.

#### **4.3 THERMAL-HYDRAULIC ANALYSIS OF THE COOLING SYSTEM FOR THE BUBBLE CHAMBER**

The purpose of this analysis was to verify that the depleted uranium (DU)-target cooling system was adequate for cooling of the bubble chamber experiment. The cooling system is shown in the process and instrumentation (P/I) diagram of Figure 12. Assumptions and input to the analysis included the following:

- The performance of the existing Haskris chiller (currently located on the service floor in Building 211) is as indicated in the email from the vendor (Appendix B).
- The performance of the pump is as indicated on the manufacturer's pump curve (Appendix B).
- The performance of the plate heat exchanger is as indicated on the vendor's quote (Appendix B).
- The pressure differential of the particle filter is as indicated in the email from the vendor (Appendix B).
- Pressure losses through the valves, pipe, and tube are calculated using data from the AFT FATHOM Version 7.0 library. Note: In general these data are in good agreement with those presented in reference [4].
- The flow channel configuration in the bubble chamber is as shown on the assembly and part drawings.
- The expansion tank is vented to atmospheric pressure.
- Required heat removal from the bubble chamber by the cooling system is 20 kW as taken from Monte Carlo particle transport code calculations (MCNPX).

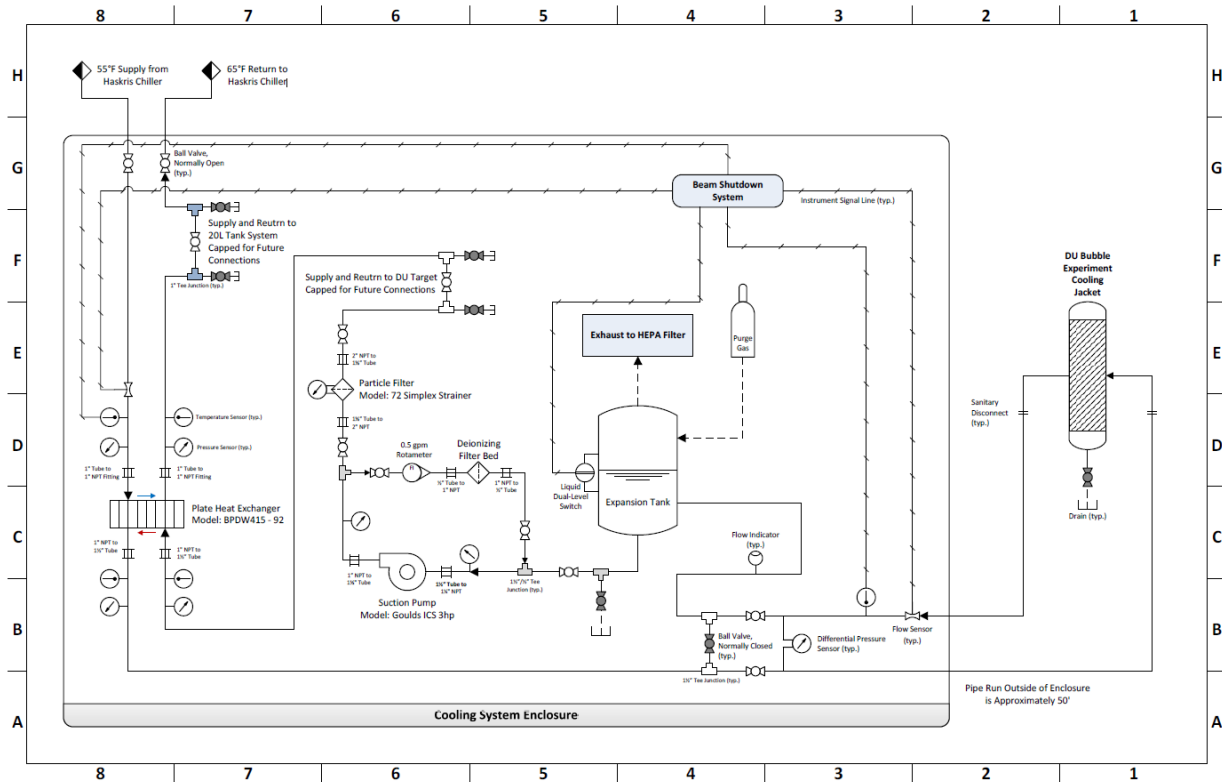


**FIGURE 12 P/I Diagram for the Bubble Chamber Cooling System**

- Flow rate through the bubble chamber is 50 gpm with a maximum inlet temperature of 70°F as required by the thermal-hydraulic analysis for the bubble chamber (Appendix B).
- Flow through the system will be manually balanced at startup, and under normal operation the flow will remain essentially constant without feedback control.
- The temperature of the system will be controlled by the constant temperature of the coolant out of the Haskris chiller (55°F). As a result, the temperature of the coolant in the primary system will be allowed to vary depending upon the heat load up to a maximum inlet temperature of 70°F at the bubble chamber (i.e., maximum heat load condition, 20 kW).
- The coolant fluid is deionized (DI) water

The commercial computer code AFT FATHOM, Version 7.0, was used to model the cooling system. The pipe and junction numbers used in the output are referenced on the model shown in Figure 13. The valves to the DU target, J27 and J28, are closed off as required by the P/I in item 1 of Appendix B. Also, valve J24 is closed to allow full flow to the bubble experiment per the P/I. The throttle valve at the discharge of the pump is 40 degrees closed to



The thermal performance of the heat exchanger, HX-1, was input from the manufacturer's data as indicated in Appendix B.

The flow channels for the bubble experiment chamber are modelled as contraction and expansion losses (i.e., area changes, J54 and J57) and rectangular tubes (P121 through P124) that have the same geometry as the flow channels in the actual chamber. Note that the heat exchanger icon for the bubble experiment is simply assigned a 20 kW heat input to the coolant with no pressure drop at that point.

The expansion tank is modeled by expansion and contraction losses (i.e., area changes, J44 and J45) into and out of tubes, P105 and P106, respectively. The tubes have the same dimensions as the actual expansion tank with J47 maintaining atmospheric pressure at J46.

The FATHOM results are shown in Appendix B. The volume flow rate through the bubble experiment chamber (J7) is indicated as 52.79 gpm, which satisfies the required minimum of 50 gpm through the chamber. The throttle valve at the discharge of the pump being set at 40% closed indicates significant additional flow capacity above the minimum that is required. Also, the temperature of the coolant entering the chamber is indicated as 68.8°F (inlet to J54), which satisfies the thermal requirement for the chamber of a maximum of 70°F. Although there is significant additional flow capacity, the reduction in inlet temperature to the chamber will be little affected by this additional increased flow. Further, considering the values shown in the FATHOM results for the tubes and fittings, all flow velocities and pressure drops are within accepted design practices. The maximum hydrostatic pressure in the system is determined by the maximum pressure at zero flow, as indicated by the pump curve in Appendix B. Therefore, assuming that the pressure in the expansion tank is always at atmospheric pressure, the maximum operating pressure of the system is 142 ft of water (61.6 psig).

## 5 MONTE CARLO SIMULATIONS

Power deposition distributions, activation of the experimental setup, and exposure rates resulting from the activated materials have been calculated to support the SHINE bubble formation experiment. This set of calculations was performed by using a general-purpose Monte Carlo particle transport code, MCNPX [5], in combination with the CINDER'90 [6] isotope transmutation package. Both codes were developed at Los Alamos National Laboratory. MCNPX tracks particle fluxes (electron/photon/neutron cascades) in various parts of the modeled geometry. CINDER'90 then uses MCNPX output (fluxes and isotope-specific material descriptions for each cell, along with the photo-nuclear reaction rates supplied by the user) and a nuclear data library for neutrons to calculate temporal densities of nuclides (both neutron- and photon-induced activation product) using the Markovian chain. The results are saved in tables stored as text files. If dose rates resulting from the activation products are the subject of interest, one more set of calculations is performed. CINDER'90 output can be parsed with "Gamma Source" Perl script (provided with the CINDER'90 package) to generate a source description for MCNPX. Subsequently, MCNPX can use this source definition to determine the dose rate distribution at different times after irradiation.

An MCNPX geometry model of the bubble formation experiment to be set up at the Low Energy Accelerator Facility (LEAF) is depicted in Figure 14. This experiment consists of a stainless-steel primary chamber that contains the DU uranyl sulfate target solution (130 g/L of uranium). Calculations were also performed for a sodium sulfate surrogate solution. Internal dimensions of the primary chamber are roughly 18 cm x 18 cm x 105 cm, and the chamber can

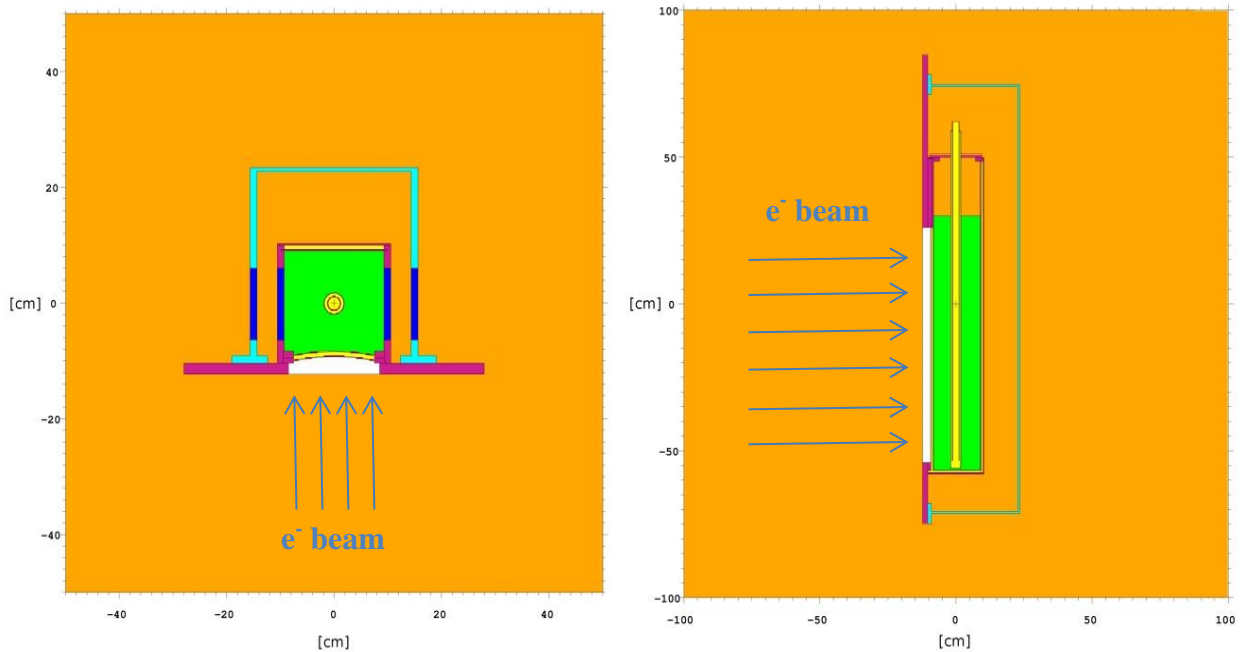


**FIGURE 14 MCNPX Geometry Model for Bubble Formation Experiment**

hold 20 L of solution. There is a double stainless-steel tube for flowing water coolant, and all equipment is encapsulated in a secondary aluminum container. Both primary and secondary chambers have quartz windows on the sides that allow observing bubble formation and dynamics with cameras during irradiation.

Figure 15 shows a spatial profile of the electron beam planned for the experiments and used in simulation studies. A horizontal double-peaked beam is rastered vertically to achieve more or less uniform irradiation of the entire target volume. The beam energy was chosen to be 35 MeV in order to achieve uniform energy deposition throughout the whole depth of the target.

## 5.1 POWER DEPOSITION DISTRIBUTIONS

Total power deposition distributions (electron/photons and neutrons) were tracked with MCNPX (using +f6 tally) and are presented in Figure 16, which shows the fractions of initial beam power deposited in each cell. This plot was generated for a sodium sulfate target solution irradiated with a 35 MeV beam. Summing up all the fractions suggests that up to 86% of the initial beam power is deposited in the experimental setup (62% in the target solution), and the rest is irradiated away by bremsstrahlung photons. Figure 17 demonstrates the forward-peaked photon flux profile in the horizontal plane per kilowatt of beam power. Since the target is irradiated with a direct electron beam, the fraction of power deposited in the solution is quite high and requires active cooling. The frame of the primary chamber also receives a significant

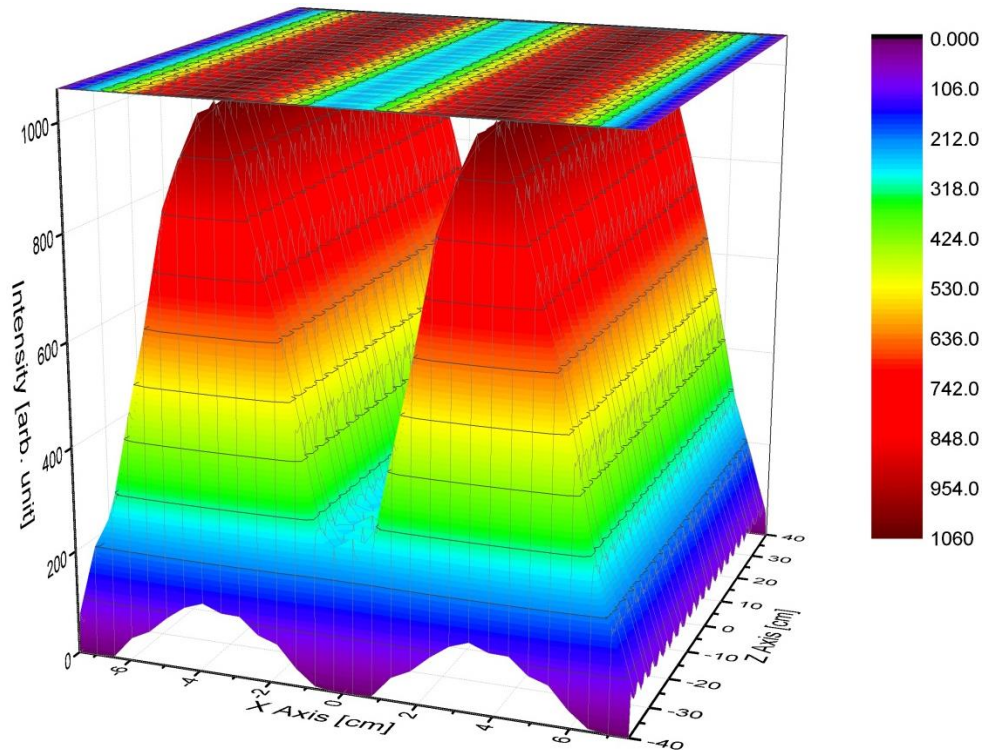


**FIGURE 15 Spatial Profile of the Electron Beam Used in MCNPX Simulations**

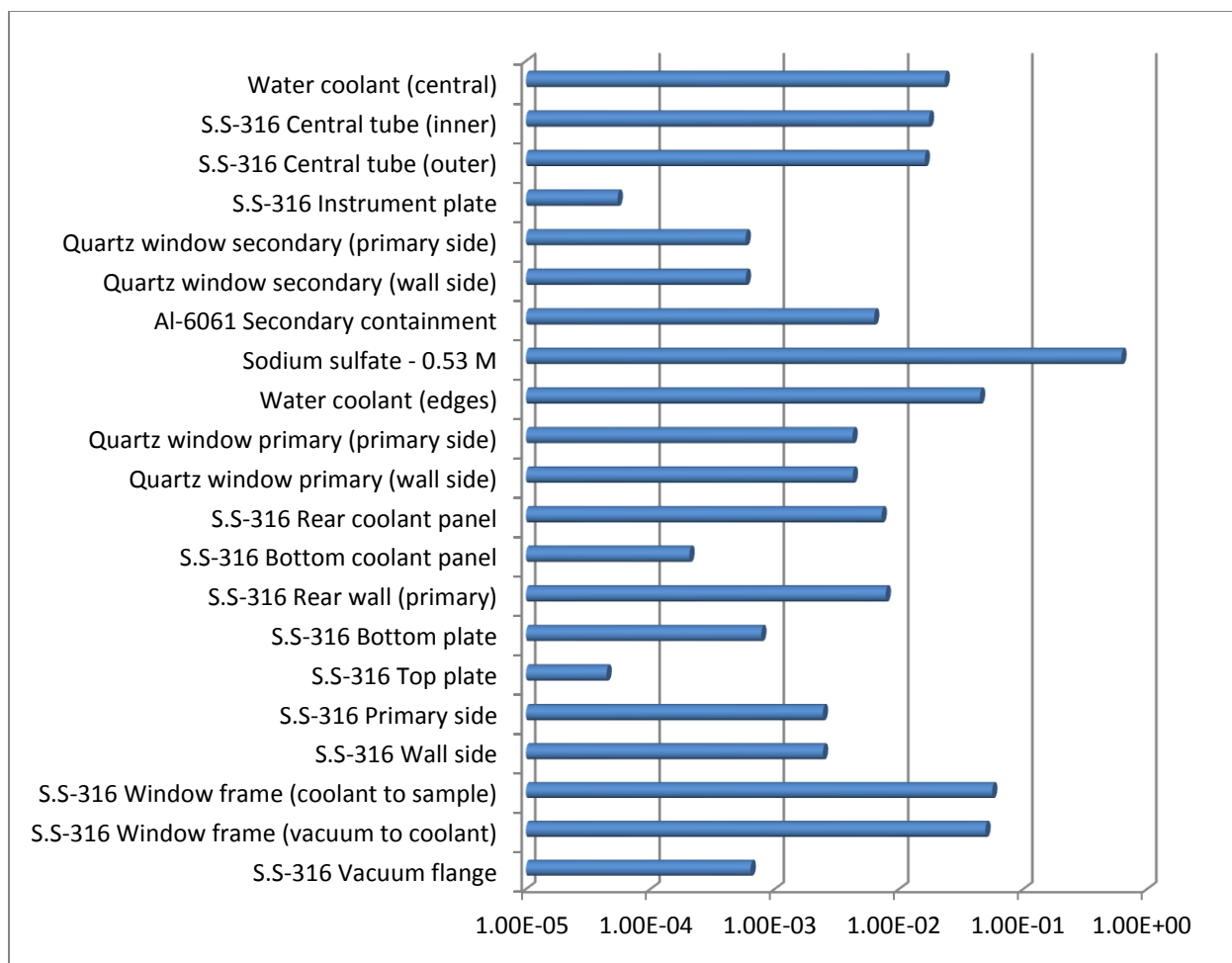


**FIGURE 16 Fractional Power Deposition in Each Cell. Modeled by MCNPX for a sodium sulfate target solution irradiated with a 35 MeV electron beam.**

portion of the beam power. For that reason, the chamber is designed to be cooled both in the middle and around the edges.

## 5.2 ACTIVATION STUDY

As already mentioned, activation calculations were performed with CINDER'90. The sodium sulfate run was done for a 20 kW beam and 4-hour irradiation, while two scenarios were considered for the uranyl sulfate run—4-hour irradiation with a 20 kW beam and 1-hour irradiation with a 10 kW beam. Photo-nuclear reaction rates were separately calculated with MCNPX based on tabulated ENDF/B-VII cross-section libraries and supplied to CINDER'90 as an input. In the case of the uranyl sulfate solution, production rates of the photo-fission residuals were obtained by applying the theoretical CEM model with MCNPX and post-processing the resulting “histp” file with CINDER'90. Activity levels of produced nuclides were calculated at 12 hours, 1 day, 2 days, 1 week, 2 weeks, and 4 weeks after the end of irradiation.



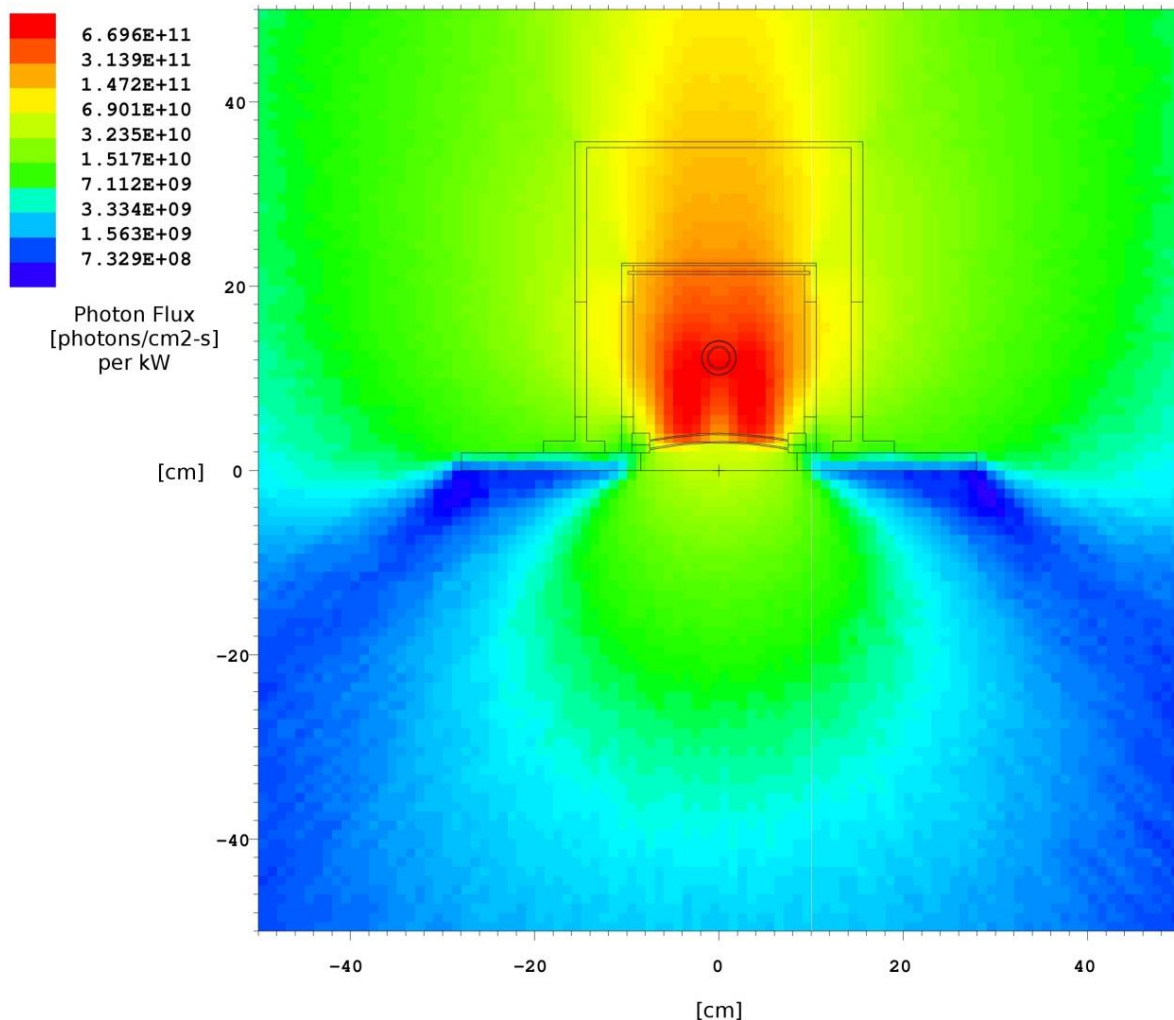


**FIGURE 17 Photon Flux Distribution per Kilowatt of Beam Power. Simulated by MCNPX for a sodium sulfate solution irradiated by a 35 MeV beam.**

Activity levels of the major activation products of the sodium sulfate surrogate solution as a function of time are shown in Figure 18. The two main gamma emitters are Na-24 and Na-22. Sodium-24 decays relatively quickly because of its 15-hour half-life, while Na-22 stays in the solution for a long time because of its 2.6-year half-life.

Total activities of each cell versus decay time were determined and plotted for the uranyl sulfate solution. Figure 19 presents these results for the case of a 10 kW beam on target for 1 hour. As expected, the total activity of the target solution dominates the other cells, with an end of burn (EOB) activity of 13 Ci. It reduces to 100 mCi in 24 hours and drops to 6 mCi at 4 weeks after irradiation.

The main driving source of the target solution activation is the photo-fission of U-238. This observation is well illustrated by Figure 20, which plots the total activity of the target uranyl sulfate cell with and without photo-fission. The plot clearly shows that photo-fission contributes



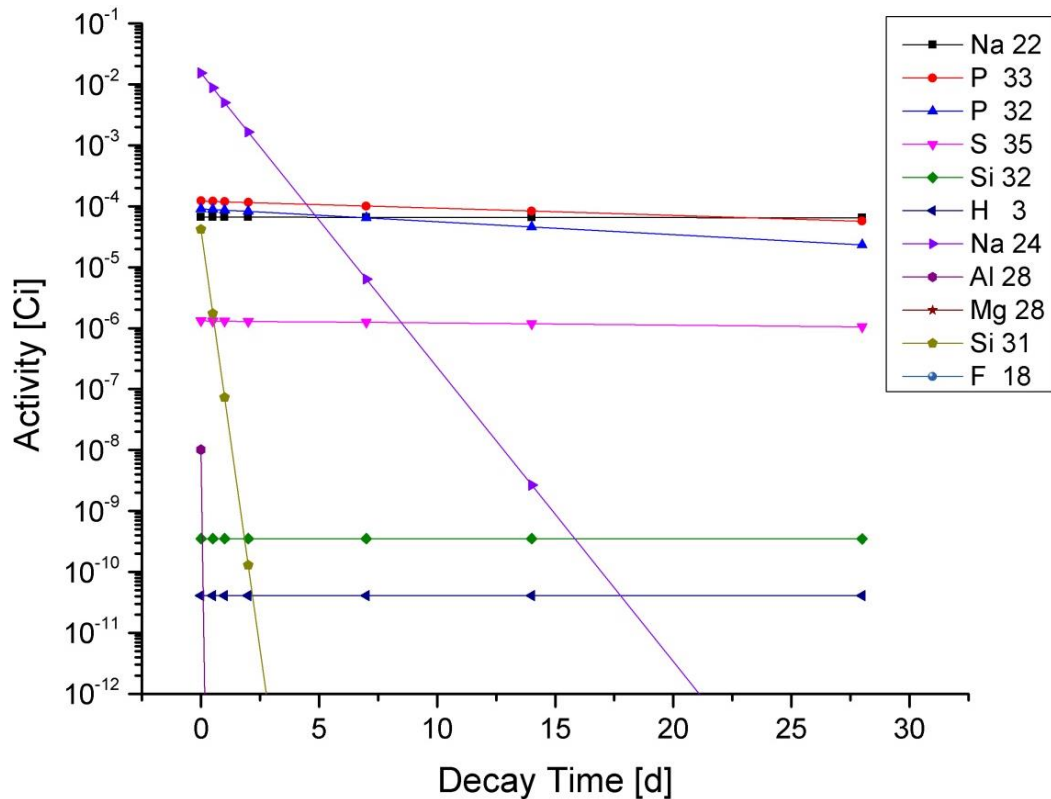


**FIGURE 18 Activity Levels of Major Activation Products in the Sodium Sulfate Solution. Generated with CINDER'90 for the case of 20 kW beam and irradiation time of 4 hours.**

more than  $\frac{3}{4}$  to the total activity. The neutron-induced fission contribution is relatively short because of the absence of a high-Z photo-neutron generator. Electrons are struck directly to a low-density target solution mostly made of low-Z elements. Because of this characteristic of the experimental setup, neutron fluxes are 3-4 orders of magnitude lower than photon fluxes, and consequently, the neutron-induced fission rates are smaller compared to the photo-induced fission rates.

### 5.3 POST-IRRADIATION EXPOSURE RATES

The MCNPX source definitions of the activated target setup were generated with the “Gamma Source” script for the following four cases: (1) sodium sulfate solution (4-hour irradiation, 20 kW beam), (2) uranyl sulfate solution (1-hour irradiation, 10 kW beam), (3) uranyl sulfate solution (4-hour irradiation, 20 kW beam) with the target solution left in the primary chamber, and (4) uranyl sulfate solution (4-hour irradiation, 20 kW beam) with the target solution drained after irradiation. Exposure rates (R/hr) were tallied at 30, 60, and 100 cm from the walls of the secondary container, both on the downstream beam axis (y-axis) and the perpendicular direction (x-axis). Exposure rate results for all four cases at 30 cm on the beam axis are presented in Figure 21.

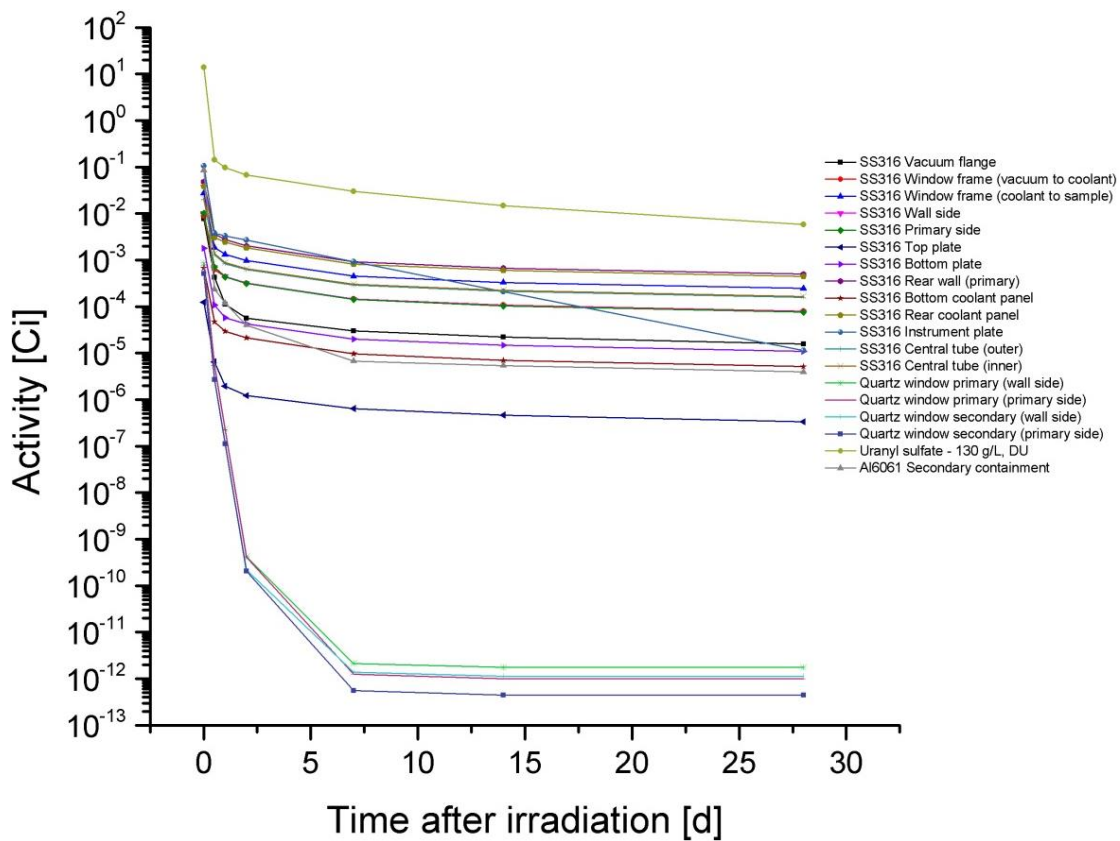


**FIGURE 19 Total Activities for Each Cell Versus Decay Time. CINDER'90 result for the uranyl sulfate solution irradiated with a 10 kW beam for 1 hour.**

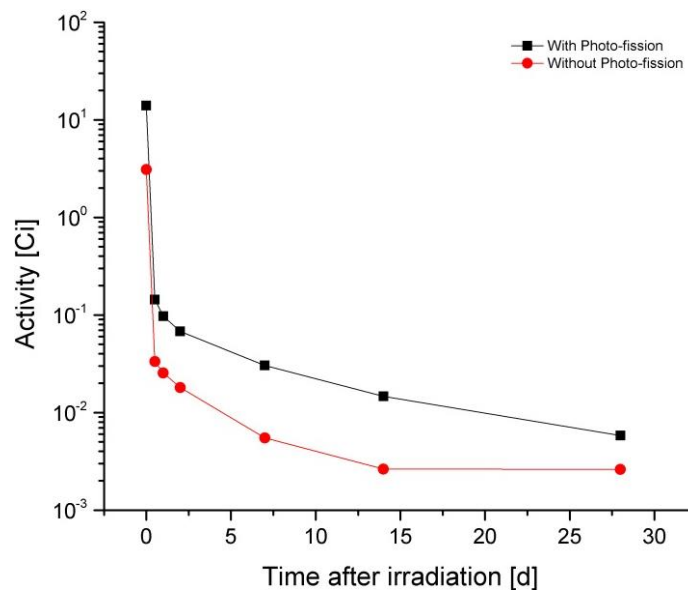


**FIGURE 20 Total Activity of the Uranyl Sulfate Target with and Without Photo-Fission**

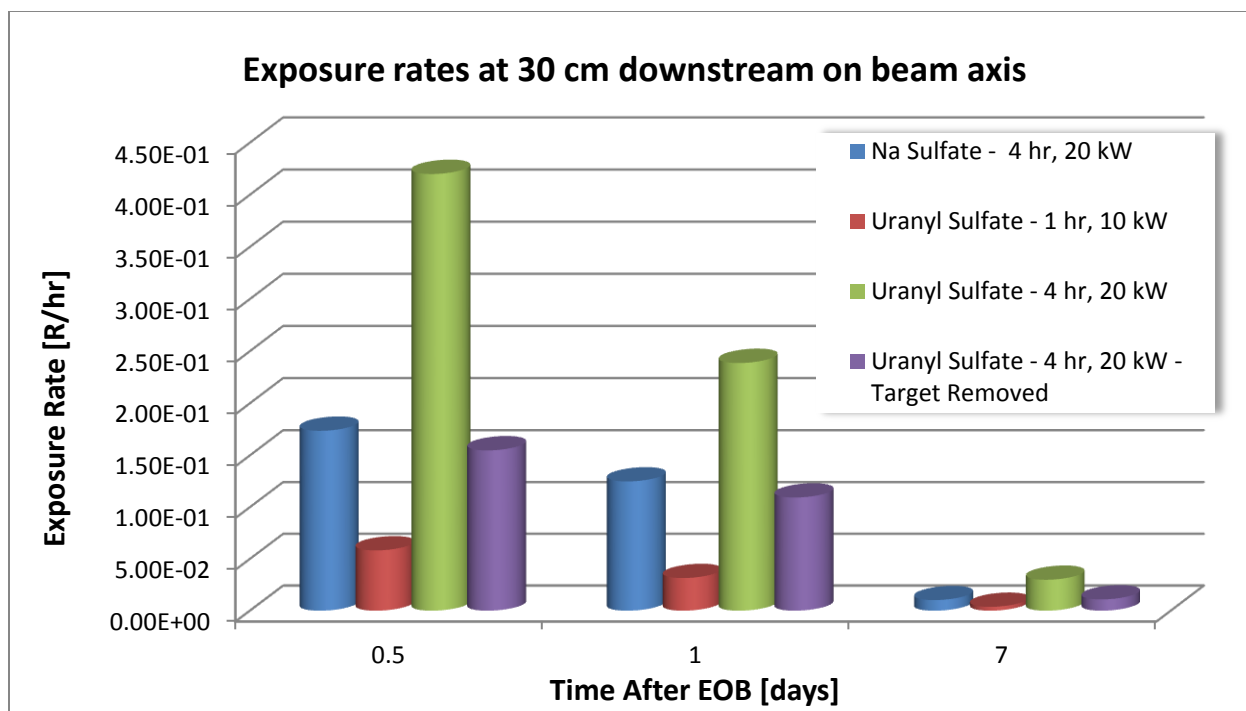


**FIGURE 21 Exposure Rate Results at 30 cm (on beam axis) for All Four Cases. Calculated with MCNPX.**

Calculations demonstrated that exposure (or dose) rates hours after irradiation scale almost linearly with irradiation time. This is why the rates for the 4-hour, 20-kW uranyl sulfate case are almost 8 times higher than the 1-hour, 10-kW case. The plot also shows that the dose rates for sodium sulfate are 2.5 times smaller than those for uranyl sulfate. Also, exposure rates with the uranyl sulfate drained from the target chamber are about 1/3 of the exposure rates with the target solution left in place. Similar results are obtained for 60 and 100 cm distances from the target enclosure. Also, it is worth noting that the exposure rates on the beam axis are higher than on the perpendicular axis due to forward-peaked nature of the bremsstrahlung photons.

## 6 PREPARATION OF THE 20-L URANYL SULFATE SOLUTION

A total of 3437 g of  $\text{U}_3\text{O}_8$  (depleted uranium) was dissolved in 150 g  $\text{U}_3\text{O}_8$  batches by adding 33 mL of concentrated  $\text{H}_2\text{SO}_4$  (Sigma-Aldrich) followed by 750 mL of 30%  $\text{H}_2\text{O}_2$  (Fisher). After the reaction was completed ( $<1$  h), the solution was heated to  $98^\circ\text{C}$  for  $\sim 4$  h to convert uranyl peroxide to uranyl sulfate. After combining the batches, the solution was brought up to  $\sim 21$  L to make  $\sim 139$  g-U/L solution. The solution was filtered using a Polycap 75 TF  $0.4\text{-}\mu\text{m}$  polytetrafluoroethylene filter capsule (Whatman). The pH of the solution is 1, measured against a pH 1 buffer solution using an Accumet AB15 Plus pH meter. The hydrogen-ion concentration was determined by taking up the uranyl sulfate solution in potassium oxalate solution (0.45 M, pH 5.54) and back-titrating with 0.1 N NaOH volumetric standard solution. From this titration, the total sulfuric acid concentration at pH 1 ( $\text{H}^+$  plus  $\text{HSO}_4^-$  concentrations) is 0.093 M.

The density of the solution was measured using a class-A 4 ( $\pm 0.01$ ) mL volumetric pipet at  $20^\circ\text{C}$  and is 1.19 g/mL. The density, plotted against data by Orban et al. [7], indicates that the concentration of uranium is 140 g-U/L. The concentration of uranium in the uranyl sulfate solution, determined by UV-V spectroscopy (Cary 5E, Varian), following a method by May et al. [8], is 129 g-U/L. The concentration of uranium determined by ICP-MS is  $128\text{ g-U/L} \pm 10\%$ . The concentration of uranium determined by HP ICP-OES, High Precision Inductively Coupled Plasma Optical Emission Spectroscopy, is  $114.25\text{ g-U/kg} \pm 0.13$ ,  $136\text{ g-U/L}$  at  $20^\circ\text{C}$ .

The purity of the solution was assayed by inductively coupled plasma mass spectroscopy (ICP-MS). The inorganic impurities found in concentrations above  $100\text{ }\mu\text{g/L}$  are (in  $\mu\text{g/L}$ ):

B	(1.8E+04)
Na	(2.48E+04)
Mg	(6.28E+05)
Al	(7.13E+03)
Si	(3.38E+04)
K	(3.07E+03)
Ti	(5.44E+04)
Cr	(1.39E+04)
Mn	(4.27E+03)
Fe	(5.64E+04)
Co	(6.26E+02)
Ni	(8.76E+04)
Cu	(2.70E+03)
Zn	(1.32E+03)
Y	(3.73E+02)
Zr	(9.67E+02)
Mo	(3.05E+03)
Sn	(1.35E+02)
Pb	(2.68E+02)

## **7 CONCLUSIONS**

This report describes the design of the bubble formation experiment and calculations performed for the design. It also records the status of the experiment as of September 23, 2014. The installation and testing are near completion, and the experiment will begin in the first half of October.

## 8 REFERENCES

- [1] Zaijing Sun, Kent Wardle, Kevin Quigley, Kent Wardle, and Sergey Chemerisov, “*Micro-Bubble Experiments at the Van de Graaff Accelerator*,” September 2014, to be published.
- [2] K. E. Wardle and H. Weller, “Hybrid Multiphase CFD Solver for Coupled Dispersed/Segregated Flows in Liquid-Liquid Extraction,” *Int. J. Chem. Eng.* 128936 (2013).
- [3] Stephen Pope, *Turbulent Flows*, Cambridge: Cambridge University Press (2000).
- [4] R. C. Binder, *Fluid Mechanics*, 3<sup>rd</sup> Edition, Englewood Cliffs, NJ: Prentice Hall (1956).
- [5] D. Pelowitz (ed.), *MCNPX User’s Manual*, Version 2.6.0, LA-CP-07-1473, Los Alamos National Laboratory (2008).
- [6] W. B. Wilson, S. T. Cowell, T. R. England, A. C. Hayes, and P. Moller, *CINDER’90 User’s Manual*, LA-UR-07-8412, Los Alamos National Laboratory (2008).
- [7] E. Orban, K. B. Martin, J. S. Boyle, J. R. Heiks, and L. V. Jones, “Physical Properties of Aqueous Uranyl Sulfate Solutions from 20 to 90°,” *J. Phys. Chem.* 60, 413-415 (1956).
- [8] I. May, S. D. Reilly, R. Copping, and D. Rios, *Uranium Measurement Control and Total Uranium Concentration Determination*, LA-UR-14-25139, Los Alamos National Laboratory (2014).

## **9 ACKNOWLEDGEMENT**

Work supported by the U.S. Department of Energy, National Nuclear Security Administration's (NNSA's) Office of Defense Nuclear Nonproliferation, under Contract DE-AC02-06CH11357. Argonne National Laboratory is operated for the U.S. Department of Energy by UChicago Argonne, LLC.

*This page intentionally left blank*



**APPENDIX A:**

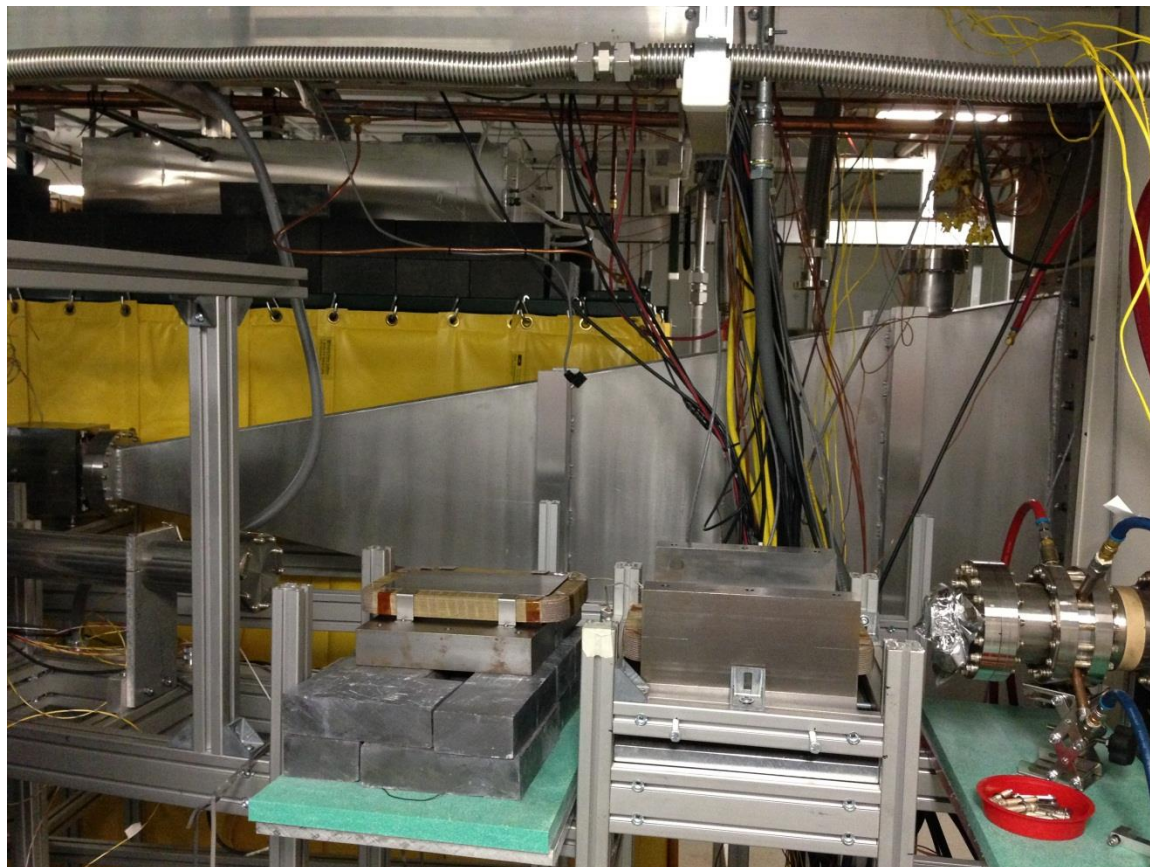
**BUBBLE CHAMBER ASSEMBLY STATUS PHOTOGRAPHS: 9-22-2014**

*This page intentionally left blank*

## APPENDIX A:

### BUBBLE CHAMBER ASSEMBLY STATUS PHOTOGRAPHS: 9-22-2014

#### Raster Magnet and Raster Chamber





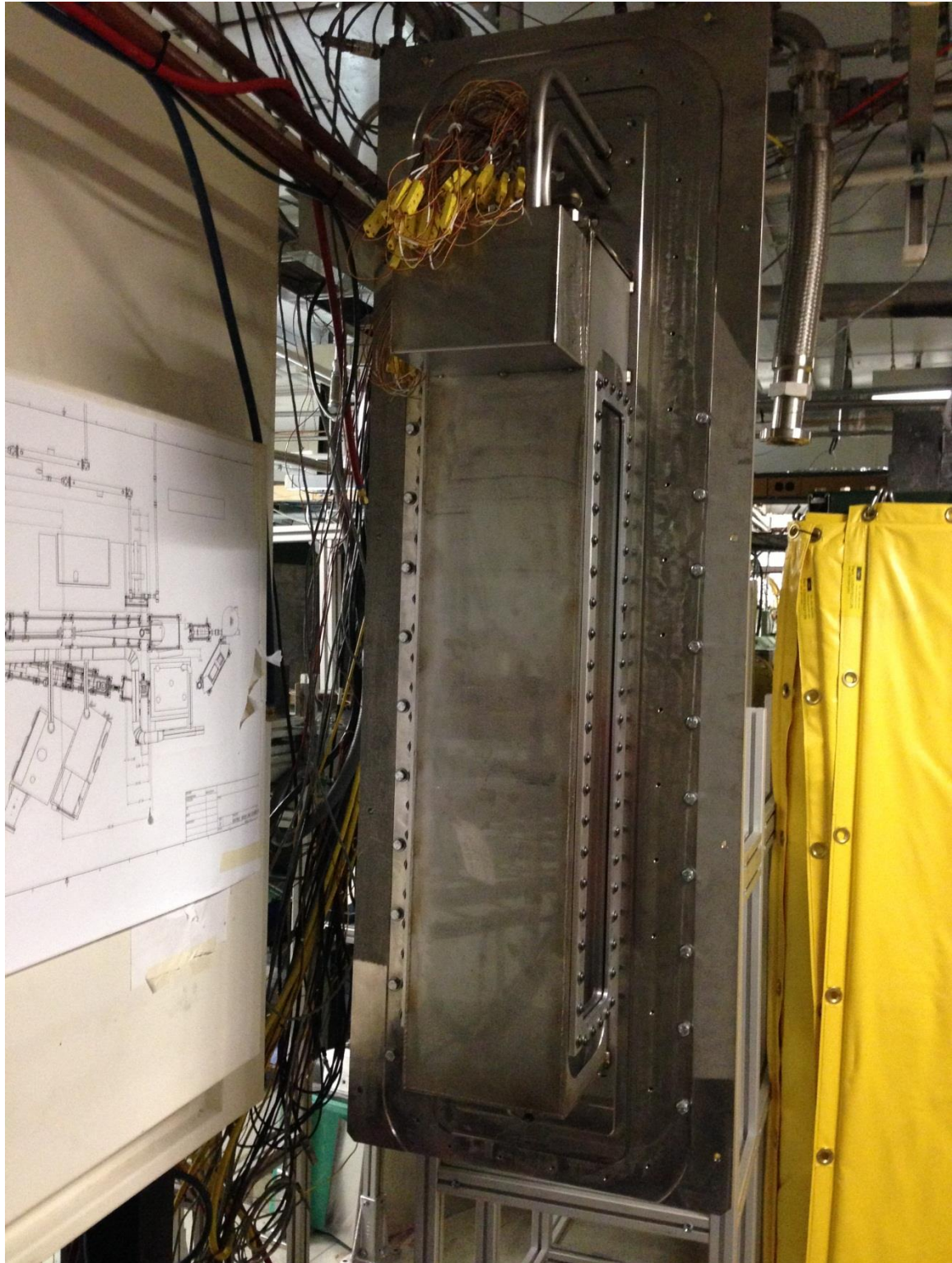


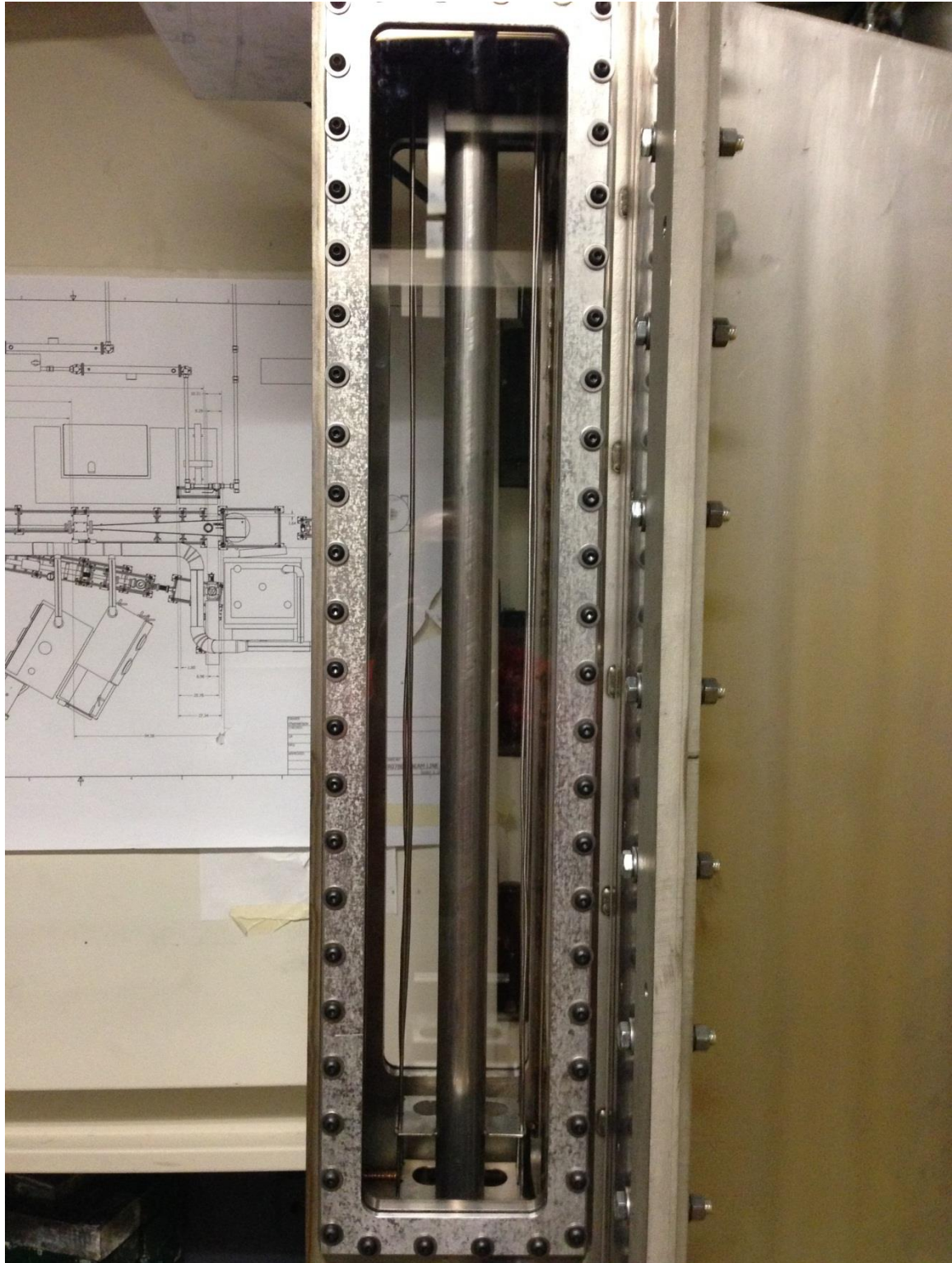


## Solution Primary Containment









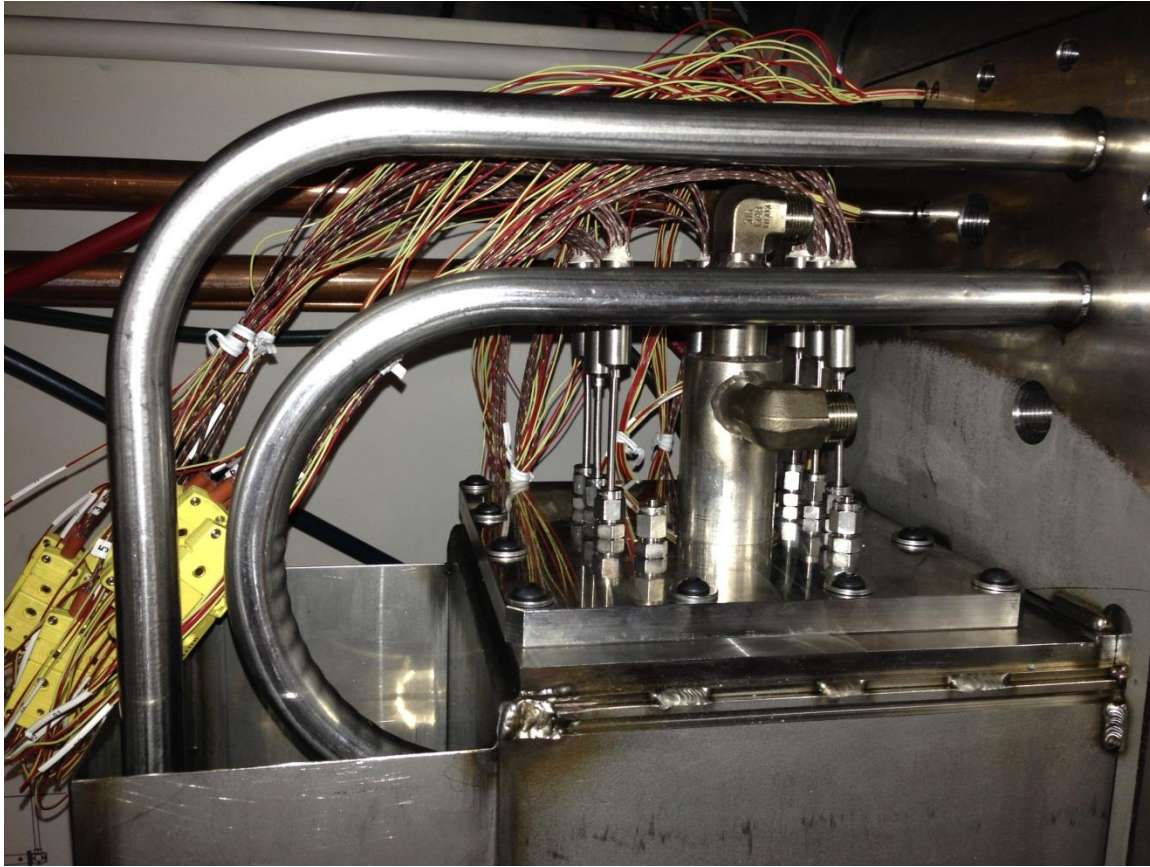






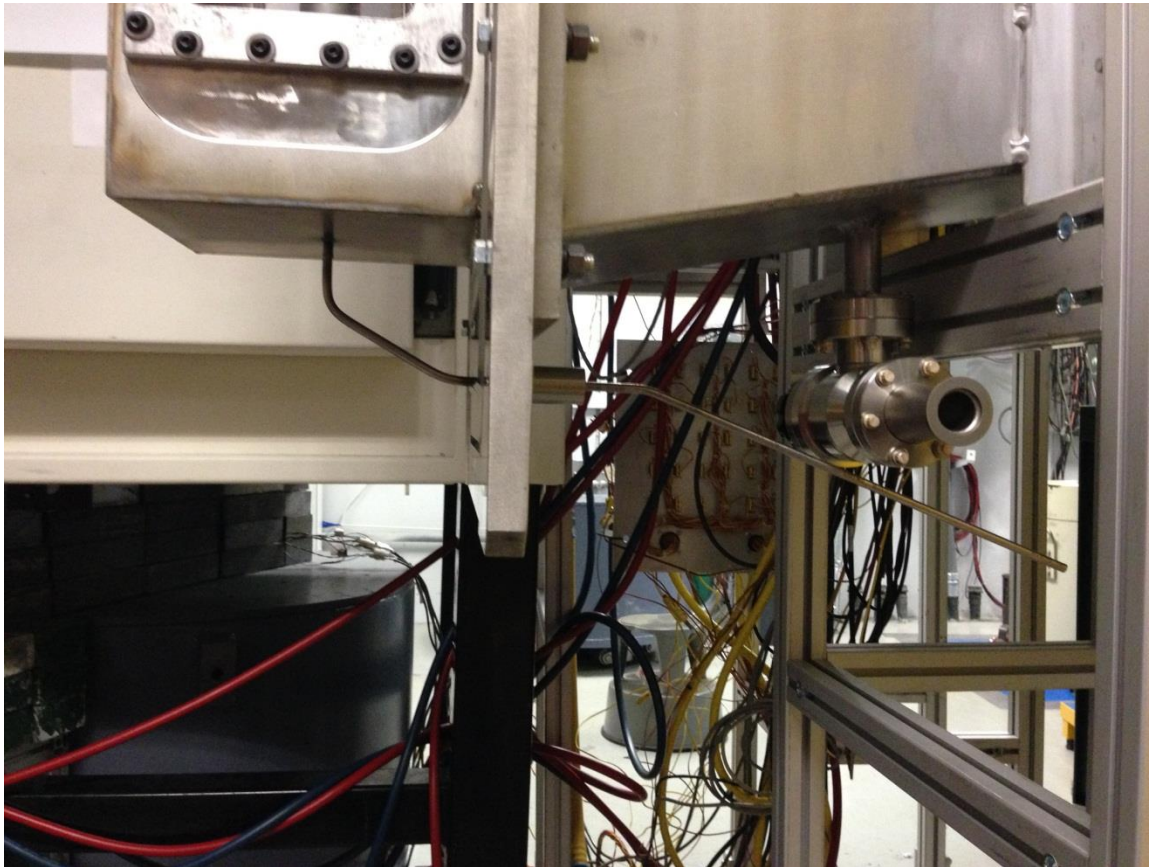


## Primary Containment Thermocouple Feedthroughs





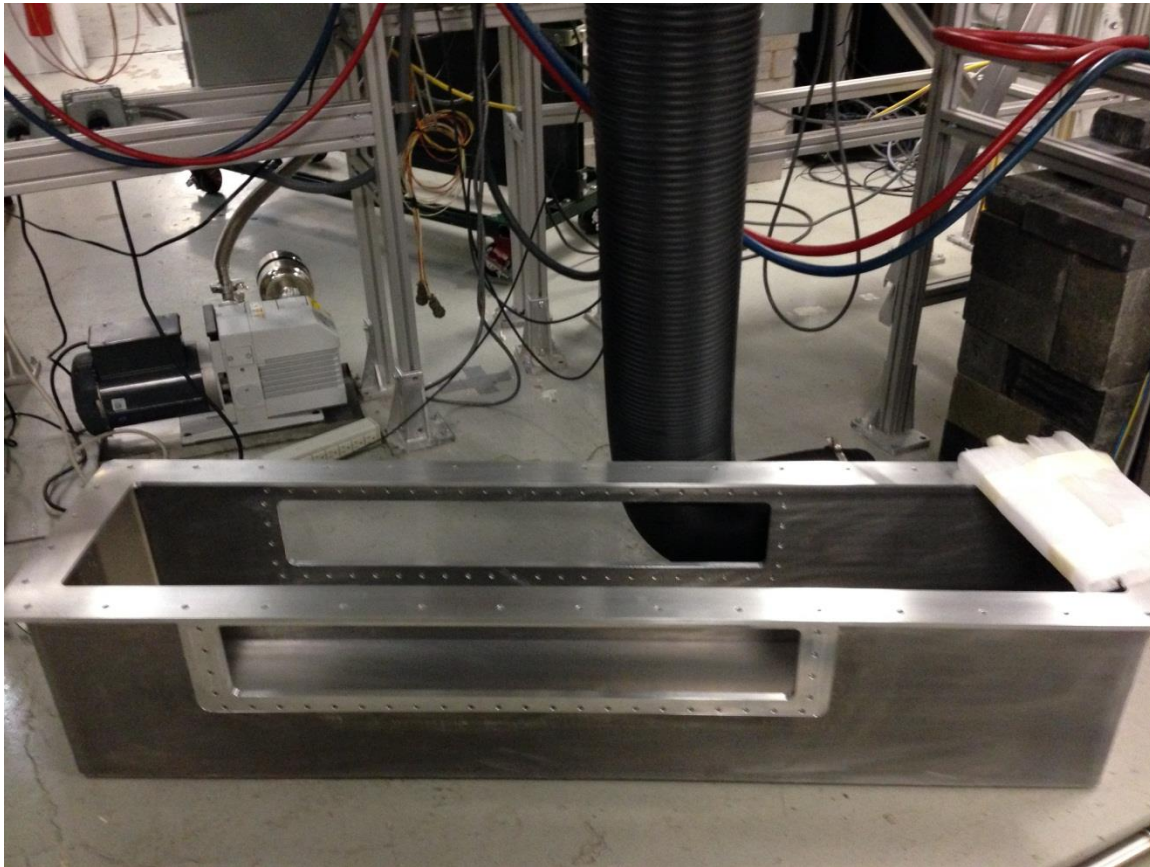
## Primary Containment Fill/Drain Line and Dump Tank

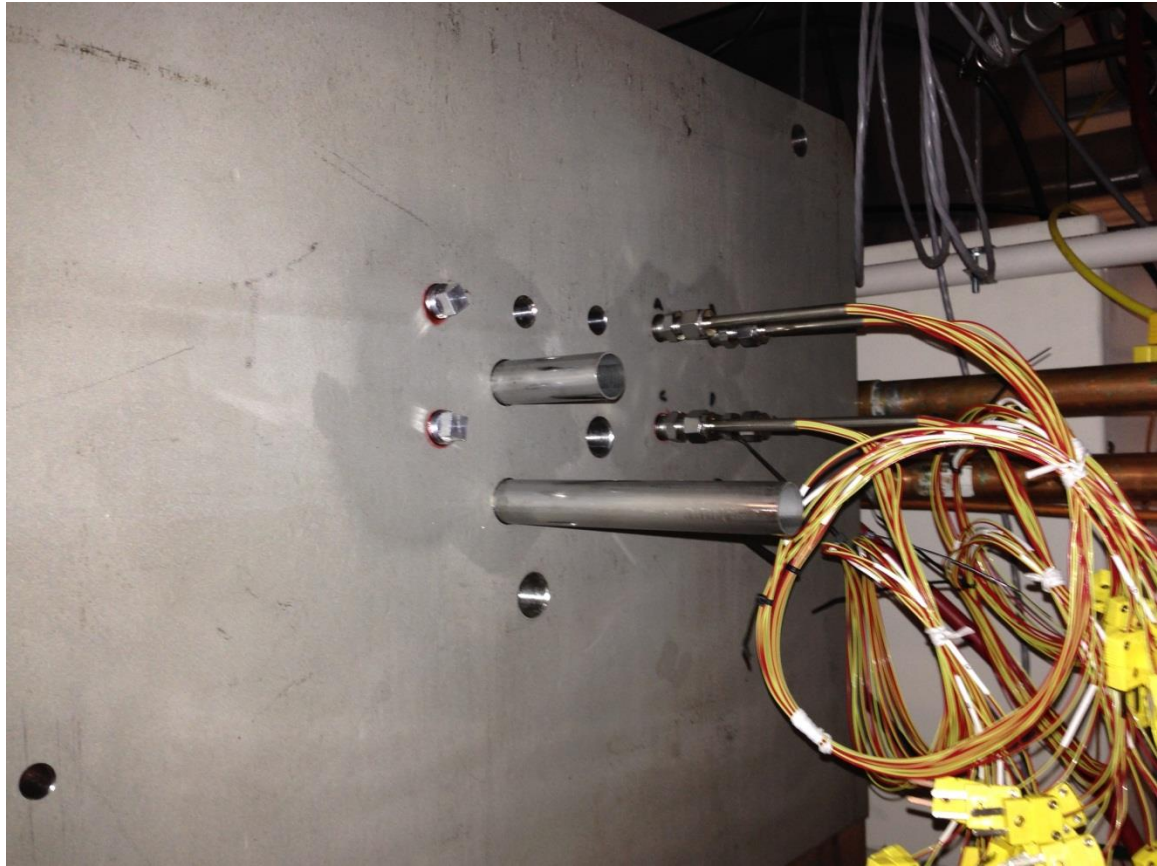






## Secondary Containment and Feedthroughs

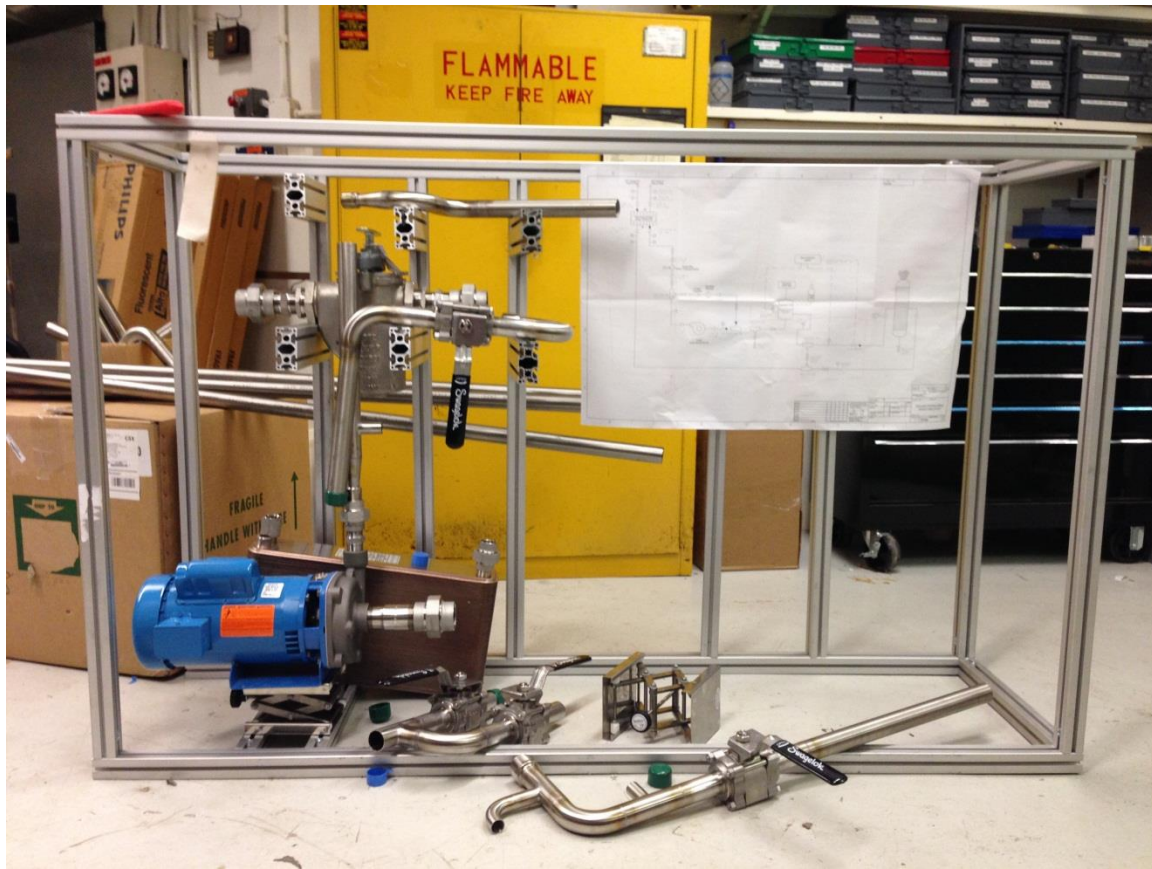






## Experiment Water Cooling System





**APPENDIX B:**  
**MECHANICAL SPEC SHEETS AND MODELLING**

*This page intentionally left blank*

## APPENDIX B:

### MECHANICAL SPEC SHEETS AND MODELLING

#### Manufacturer's Data for FATHOM Code Input

Email from the Haskris chiller manufacturer verifying performance characteristics:

Hi James,

Thank you for contacting Haskris. Attached is the manual that is sent with each of our chillers; since we build each unit to order, it only includes general installation, operation, and maintenance. Below are the specifications of the unit:

Voltage: 208/230V – 3 phase – 60Hz  
FLA = 30A  
MOCP = 40A

Maximum cooling capacity: 23kW @ 65°F supply water set-point  
Condenser: Water-cooled (heat dissipated into secondary source of water)  
Refrigerant: R22 (17lbs, 6oz)  
Water temperature connections: 65 – 69°F

Pump Capacity: 12.5GPM @ 45psi  
Tank size: 30 gallons  
Supply and return connections: 3/4" FPT Brass  
Condenser water connections: 3/4" FPT Brass

If you have any questions, please let me know.

Regards,  
Mike

**Mike Macak**  
Application Engineer  
T: (847) 956-6420 x273  
F: (847) 956-6595  
[www.haskris.com](http://www.haskris.com)  
100 Kelly St. | Elk Grove Village, IL 60007 | USA

#### Gould pump information

Good afternoon Jim,

Please see the quotation below per your request. If you have any questions or need any additional assistance please let me know!

Reference Quotation Number: UQ0414308

QTY(1) 1SS1H4A0, Goulds model ICS

- 1 X 1-1/4 - 5
- 316SS
- 3HP, 3500RPM
- 60Hz/1PH/TEFC
- 5-3/8" Impeller Diameter
- Carbon/Silicon Carbide/Viton Mechanical Seal
- Your net price each: \$1,989.00
- Typically ships in about 7-10 Days

**\*Prices quoted are net\***

**\*Quotation is valid for 30 Days\***

**\*Freight: Pre-Pay & Add or Collect, FOB: Shipping Point\***

**\*Xylem, Inc. standard terms & conditions apply\***

Thanks for the opportunity,

***Mark Nelson***

Mack Pump & Equipment Co., Inc.  
Office: 815-439-2030  
Fax: 815-439-2451  
E-mail: [mnelson@mackpump.com](mailto:mnelson@mackpump.com)

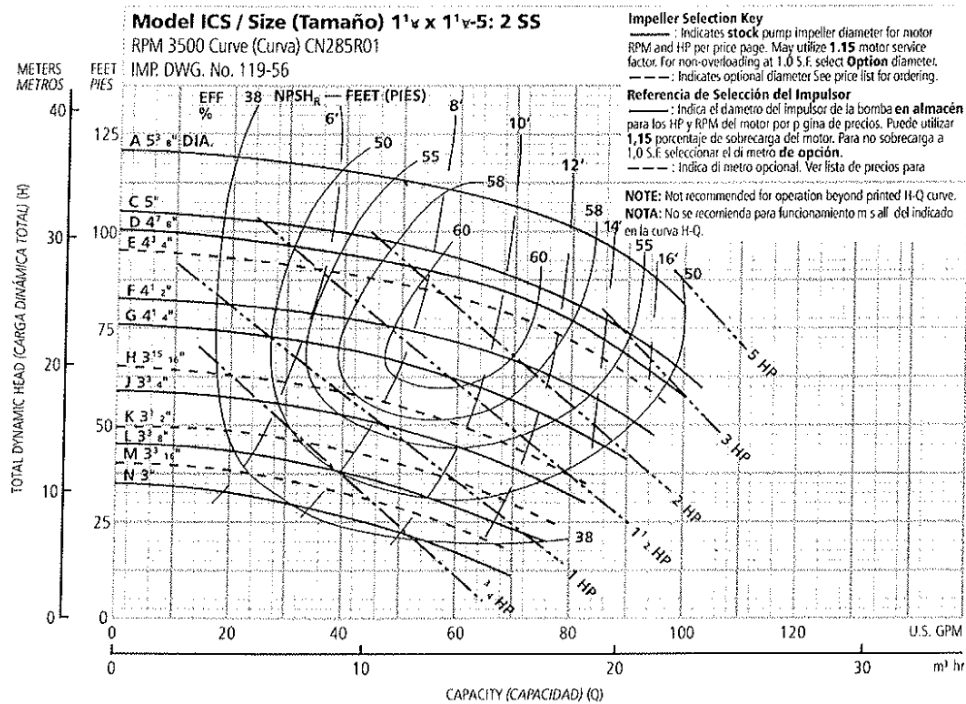


## Plate heat exchanger information



7050 N. LEHIGH AVE. CHICAGO, IL 60646  
 PHONE (773) 774-2800/FAX (773) 763-6534  
 e-mail: bornquist@bornquist.com  
 website: www.bornquist.com

MANUFACTURERS  
 REPRESENTATIVES

Quotation No. SA 2014-4-29-10.04	
Quote Date:	4/29/2014
Date:	4/29/2014 2:02:11 PM
Terms:	
Freight:	Freight Prepaid and Add
Job:	ARGONNE LAB HEAT EXCHANGER
TO:	
ATTN:	Engineer: None Selected

We are pleased to quote you on the following equipment for the above job subject to approval. Quantities listed are not guaranteed and should be verified. Prices will be adjusted accordingly. This quotation is subject to change without notice and void after 30 days unless otherwise stated below. All Contracts or Orders are subject to acceptance by the Company and are contingent upon non-occurrence of strikes or other delays beyond their control. In addition to prices named herein, you are to pay any applicable sales taxes.

Qty	Description & Tag	Wt (lbs)	Net Price Ea.	Total Net Price
1	<b>BRAZED PLATE HEAT EXCHANGERS</b>  B&G Model - BPDW415 - 92 Plate Heat Exchanger - Consisting of a Brazed Pack Unit with 92 Plates. Thermal Plates are SA240 S31603 X 0.0157 in. tk. This unit has the following connections: Port-1: 1" NPT Male Thread, Port-2: 1" NPT Male Thread, Port-3: 1" NPT Male Thread, Port-4: 1" NPT Male Thread, Working Pressure: 435 psig. Mounting Options: , ASME CODE: NO. Hot Side: 50 GPM of Water from 67 F to 65 F with 10 psi pressure drop; Cold Side: 10 GPM of Water from 55 F to 65 F.	101	\$3,682.00	\$3,682.00
	<b>Total BRAZED PLATE HEAT EXCHANGERS</b>			\$3,682.00

Model	Plates	Passes (H)	Passes (C)	Area (ft2)	U Value (Btu/hr.ft2.°F)	P Drop H/S(Psi)	P Drop C/S(Psi)	Stock Unit	Weight (lb)	*Price Factor	Lead Time
BPDW415 - 92	92	1	1	48.24	439.99	9.92	0.39	NO	101.04	1.00	10 days

Selection Details

## Particle filter information 2" Model 72 Simplex

Jim,

Understand your question , but Eaton decided years ago to standardize their ½" through 2" sizes around a 600# ANSI class to cover most steam applications. There is no lower pressure version offered, and the initial request was for the Y-strainer so the model 85 was quoted, however , we can certainly go to a basket strainer , model 72 Simplex that would have a 0.7 psi initial clean drop at 50 gpm fitted with a 60 mesh screen. Reason is that a 2" model 72 Simplex basket has about 51 sq. in. of gross screen area whereas the Y-strainer has 30.4. The model 72 is also easier for maintenance. Only drawback is that it's not standardly offered with socket weld connections. I'm assuming the pipe run is horizontal , necessary for the model 72.

The part # for the 316 SS 2" NPT #72 is ST0720200T2C..... 200 PSIG @ 100 deg. F, 2" NPT , Viton seal and includes one 316 SS 60 mesh lined basket.....\$ 991.00 net each , same 3 to 5 day lead time to ship.

Support data attached. The appropriate curve for the 72 is at the bottom half of page one of the 'Curves' attachment.

Regards,  
Dave Natalino  
Pargreen Process Technologies  
1224 Capitol Dr.  
Addison, IL, 60101  
Ph. # 630-628-1330  
Fax# 630-628-3050

[dnatalino@pargreen.com](mailto:dnatalino@pargreen.com)



## Input to the components in the FATHOM Model

**Pump Specifications**

Number: 6 Upstream Pipe: 125  
Name: Pp-1 Gould Centrifugal Pump Downstream Pipe: 111  
Database List: Elevation  
Copy Data From Jct... Inlet: 1 feet  
Outlet: Same as Inlet NPSH Reference:

OK Cancel Jump... Help

Pump Model | Variable Speed | Thermal | Optional | Cost | Notes | Status

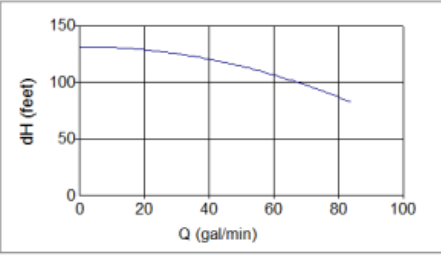
Pump Model

☒ Pump Curve Enter Curve Data...  
☐ Volumetric Flow Rate Fixed  
☐ Mass Flow Rate Fixed  
☐ Head Rise Fixed  
☐ Pressure Rise Fixed

Impeller Modifications  
☐ Ratio as Percent  
☐ Actual Impeller Trim inches

☐ Check Valve at Discharge (No Backflow Allowed)

Max X-Axis Value: 84 Update Graph



Head Rise | NPSHR | Efficiency | Parameters and Constants

### Pump curve

**General Component Specifications**

Number: 41 Upstream Pipe: 72  
Name: Particulate Filter Downstream Pipe: 73  
Database List: Elevation  
Copy Data From Jct... Inlet: 1 feet  
Outlet: Same as Inlet

OK Cancel Jump... Help

Loss Model | Optional | Notes | Status

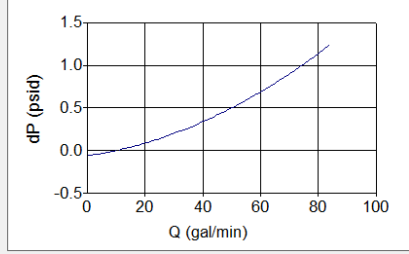
Loss Model

☐ K Factor (Constant)  
☐ K Factor (Variable)  
☒ Resistance Curve Enter Curve Data...

Basis Area for Loss Model  
Upstream Pipe

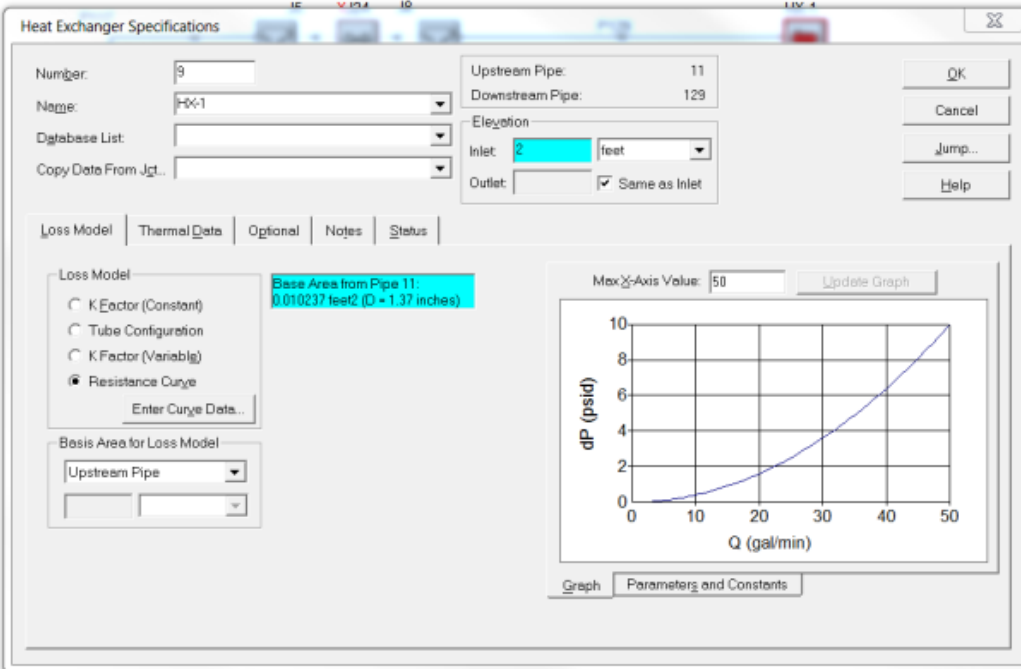
Base Area from Pipe 72:  
0.010237 feet<sup>2</sup> (D = 1.37 inches)

Max X-Axis Value: 84 Update Graph



Graph | Parameters and Constants

### Pressure drop curve for the Particle Filter



Heat Exchanger Hydraulic Performance Curve

The dialog box displays the following settings:

- Number: 9
- Name: HX-1
- Database List: (empty)
- Copy Data From Jct.: (empty)
- Upstream Pipe: 11
- Downstream Pipe: 129
- Elevation: Inlet: 2 feet, Outlet: (empty), Same as Inlet: checked

The Thermal Model section shows:

- Thermal Model: Parallel
- Link to Heat Exchanger: (empty)
- Heat Flow Into System: (empty) Btu/s
- Controlled Outlet Temperature: (empty) deg. F
- Heat Transfer Area: 48.24 feet<sup>2</sup>
- Overall Heat Transfer Coefficient: 439.99 Btu/hr-ft<sup>2</sup>-R
- Secondary Fluid Data:
  - Flow Rate: 83.4 lbm/min
  - Specific Heat: 1 Btu/lbm-R
  - Inlet Temperature: 55 deg. F

Heat Exchanger Thermal Performance

**Valve Specifications**

Number: 10  
 Name: Throttle Valve  
 Database List:  
 Copy Data From Jgt...  
 Upstream Pipe: 114  
 Downstream Pipe: 72  
 Elevation  
 Inlet: 1 feet  
 Outlet: ☒ Same as Inlet

Loss Model | Optional | Notes | Status

Valve Data Source  
☒ Handbook Data  
 Ball, 40 deg. (I)  
☐ User Specified

Handbook Database List Definitions  
 Abbreviations:  
 D= Diameter AR= Area Ratio (C)= Crane  
 PO= Percent Open deg.= degrees (I)= Idelchik  
 (M)= Miller

Loss Model  
☐ Cv (Constant)  
☒ K Factor (Constant)  
☐ K Factor (Variable)  
☐ Resistance Curve

Cv Data  
☒ User Specified  
☐ From % Open Table (on Optional tab)

K: 9.2

Basis Area for Loss Model  
 Upstream Pipe  
 Base Area from Pipe 114:  
 0.010237 feet<sup>2</sup> (D = 1.37 inches)

☐ Exit Valve (optional)  
☐ Head (HGL) Exit Pressure:  
☐ Pressure Exit Temperature: deg. F

OK  
 Cancel  
 Jump...  
 Help

### Throttle Valve at Discharge of Pump

**Valve Specifications**

Number: 51  
 Name: Valve  
 Database List:  
 Copy Data From Jgt...  
 Upstream Pipe: 109  
 Downstream Pipe: 113  
 Elevation  
 Inlet: 1 feet  
 Outlet: ☒ Same as Inlet

Loss Model | Optional | Notes | Status

Valve Data Source  
☒ Handbook Data  
 Ball, 70 deg. (I)  
☐ User Specified

Handbook Database List Definitions  
 Abbreviations:  
 D= Diameter AR= Area Ratio (C)= Crane  
 PO= Percent Open deg.= degrees (I)= Idelchik  
 (M)= Miller

Loss Model  
☐ Cv (Constant)  
☒ K Factor (Constant)  
☐ K Factor (Variable)  
☐ Resistance Curve

Cv Data  
☒ User Specified  
☐ From % Open Table (on Optional tab)

K: 204

Basis Area for Loss Model  
 Upstream Pipe  
 Base Area from Pipe 109:  
 7.47E-04 feet<sup>2</sup> (D = 0.37 inches)

☐ Exit Valve (optional)  
☐ Head (HGL) Exit Pressure:  
☐ Pressure Exit Temperature: deg. F

OK  
 Cancel  
 Jump...  
 Help

### Valve in the DI Bypass Line for Throttling Flow through the DI Unit

## Results from the FATHOM Model (Note that the input for tube size and lengths are also noted here)

Pipes		Heat Transfer																
Pipe	Name	Vol. Flow Rate (gal/min)	Velocity (feet/sec)	Elevation Inlet (feet)	Elevation Outlet (feet)	dP Stag. Total (psid)	dP Static Total (psid)	dP Gravity (psid)	P Static In (psig)	P Static Out (psig)	P Stag. In (psig)	P Stag. Out (psig)	T Inlet (deg F)	T Outlet (deg F)	f	Pipe Nominal Size	Length (feet)	
11	Pipe	52.807	11.4931	1.000	2.000	0.703241	0.703241	0.4326	37.9896927	37.2864532	38.877769	38.1745	71.42	71.42	0.01739	1-1/2 inch	2.0000	
12	Pipe	52.807	11.4931	1.000	1.000	0.135309	0.135309	0.0000	38.1250038	37.9896927	39.013081	38.8778	71.42	71.42	0.01739	1-1/2 inch	1.0000	
13	Pipe	52.807	11.4931	1.000	1.000	0.135309	0.135309	0.0000	38.2780762	38.1427650	39.166153	39.0308	71.42	71.42	0.01739	1-1/2 inch	1.0000	
16	Pipe	0.000	0.0000	5.000	5.000	0.000000	0.000000	0.0000	2.1097202	2.1097202	2.109720	2.1097	71.41	71.41	0.00000	1-1/2 inch	1.0000	
17	Pipe	0.000	0.0000	5.000	5.000	0.000000	0.000000	0.0000	24.9047318	24.9047318	24.904732	24.9047	68.82	68.82	0.00000	1-1/2 inch	1.0000	
19	Pipe	52.824	11.4968	5.000	1.000	-1.188928	-1.188928	-1.7305	-0.8962631	0.2926645	-0.007622	1.1813	71.42	71.42	0.01739	1-1/2 inch	4.0000	
72	Pipe	52.807	11.4931	1.000	1.000	0.135309	0.135309	0.0000	39.2518692	39.1165581	40.139946	40.0046	71.42	71.42	0.01739	1-1/2 inch	1.0000	
73	Pipe	52.807	11.4931	1.000	1.000	0.135309	0.135309	0.0000	38.5664558	38.4311447	39.454533	39.3192	71.42	71.42	0.01739	1-1/2 inch	1.0000	
91	Pipe	52.807	11.4931	5.000	5.000	0.135314	0.135314	0.0000	1.3569584	1.2216463	2.245033	2.1097	71.41	71.41	0.01740	1-1/2 inch	1.0000	
92	Pipe	52.807	11.4931	5.000	5.000	8.118840	8.118840	0.0000	9.4935608	1.3747215	10.381636	2.2628	71.41	71.41	0.01740	1-1/2 inch	60.0000	
93	Pipe	52.790	11.4895	5.000	5.000	8.172958	8.172958	0.0000	23.8629608	15.6900024	24.750759	16.5778	68.82	68.82	0.01752	1-1/2 inch	60.0000	

94	Pipe	52.790	11.4895	5.000	5.000	0.136216	0.136216	0.0000	24.0169334	23.8807144	24.904732	24.7685	68.82	68.82	0.01752	1-1/2 inch	1.0000
101	Pipe	0.000	0.0000	0.000	1.000	0.432622	0.432622	0.4326	39.3103943	38.8777695	39.310394	38.8778	71.42	71.42	0.00000	1 inch	2.0000
102	Pipe	0.000	0.0000	0.000	0.000	0.000000	0.000000	0.0000	No Solution	No Solution	No Solution	No Solution	No Solution	No Solution	0.00000	1 inch	2.0000
103	Pipe	0.000	0.0000	0.000	0.000	0.000000	0.000000	0.0000	No Solution	No Solution	No Solution	No Solution	No Solution	No Solution	0.00000	1 inch	2.0000
104	Pipe	0.000	0.0000	1.000	0.000	-0.432622	-0.432622	-0.4326	39.1661530	39.5987740	39.166153	39.5988	71.42	71.42	0.00000	1 inch	2.0000
105	Pipe	52.807	0.1405	6.000	6.000	0.001278	0.001278	0.0000	-0.0014105	-0.0001326	-0.001278	0.0000	71.41	71.41	0.02837	12 inch	0.2500
106	Pipe	52.824	0.1406	6.000	5.000	-0.432618	-0.432618	-0.4326	-0.0001326	0.4324856	0.000000	0.4326	71.42	71.42	0.02837	12 inch	1.2500
107	Pipe	0.000	0.0000	6.000	6.000	0.000000	0.000000	0.0000	0.0000000	0.0000000	0.000000	0.0000	65.00	65.00	0.00000	1/2 inch	1.0000
109	Pipe	1.927	5.7487	1.000	1.000	0.196099	0.196099	0.0000	46.9589462	46.7628479	47.181126	46.9950	71.42	71.42	0.02721	1/2 inch	1.0000
111	Pipe	54.734	11.9125	1.000	1.000	0.144384	0.144384	0.0000	47.6363297	47.4919472	48.590405	48.4460	71.42	71.42	0.01728	1-1/2 inch	1.0000
112	Pipe	1.927	5.7487	1.000	1.000	0.196099	0.196099	0.0000	1.2034254	1.0073271	1.425606	1.2295	71.42	71.42	0.02721	1/2 inch	1.0000

113	Pipe	1.927	5.7487	1.000	1.000	0.196099	0.196099	0.0000	1.4380569	1.2419558	1.660236	1.4641	71.42	71.42	0.02721	1/2 inch	1.0000
114	Pipe	52.807	11.4931	1.000	1.000	0.135309	0.135309	0.0000	47.5574722	47.4221649	48.445549	48.3102	71.42	71.42	0.01739	1-1/2 inch	1.0000
115	Pipe	52.807	11.4931	1.000	1.000	0.135309	0.135309	0.0000	38.4133835	38.2780762	39.301460	39.1662	71.42	71.42	0.01739	1-1/2 inch	1.0000
117	Pipe	52.807	11.4931	5.000	6.000	1.244507	1.244507	0.4326	1.2216463	-0.0228605	2.109720	0.8652	71.41	71.41	0.01740	1-1/2 inch	6.0000
120	Pipe	1.927	5.7487	1.000	1.000	0.196150	0.196150	0.0000	1.0028830	0.8067331	1.225063	1.0289	71.42	71.42	0.02721	1/2 inch	1.0000
121	Pipe	52.790	8.7416	5.000	5.000	0.965298	0.965298	0.0000	14.2882862	13.3229866	14.802204	13.8369	68.82	68.82	0.02333	None	3.2500
122	Pipe	52.790	8.7416	5.000	5.000	0.096035	0.096035	0.0000	12.6841640	12.5881290	13.198082	13.1020	68.82	68.82	0.02333	None	0.3233
123	Pipe	52.807	8.7443	5.000	5.000	0.095302	0.095302	0.0000	12.5879707	12.4926682	13.102047	13.0067	71.41	71.41	0.02314	None	0.3233
124	Pipe	52.807	8.7443	5.000	5.000	0.957934	0.957934	0.0000	11.8536472	10.8957138	12.367723	11.4098	71.41	71.41	0.02314	None	3.2500
125	Pipe	54.734	11.7405	1.000	1.000	0.156039	0.156039	0.0000	-0.0423775	-0.1984158	0.884342	0.7283	71.42	71.42	0.01936	1-1/4 inch	1.0000
126	Pipe	54.734	11.9125	1.000	1.000	0.144372	0.144372	0.0000	0.0748386	-0.0695333	1.028913	0.8845	71.42	71.42	0.01728	1-1/2 inch	1.0000

128	Pipe	52.824	11.4968	1.000	1.000	0.134620	0.134620	0.0000	0.2748919	0.1402721	1.163533	1.0289	71.42	71.42	0.01739	1-1/2 inch	1.0000
129	Pipe	52.790	11.4895	2.000	5.000	2.115567	2.115567	1.2983	26.1324997	24.0169334	27.020298	24.9047	68.82	68.82	0.01752	1-1/2 inch	6.0000

Jct	Name	P Static In (psig)	P Static Out (psig)	Vol. Flow Rate Thru Jct (gal/min)	T Inlet (deg. F)	T Outlet (deg. F)	P Stag. In (psig)	P Stag. Out (psig)
1	Valve	23.88071442	23.86296082	52.790	68.82	68.82	24.7685	24.750759
2	Valve	1.37472153	1.35695839	52.807	71.41	71.41	2.2628	2.245033
5	Tee or Wye	1.71510124	1.71510124	N/A	71.41	71.41	2.1097	2.109720
6	Pp-1 Gould Centrifugal Pump	-0.19841576	47.63632965	54.734	71.42	71.42	0.7283	48.590405
7	Bubble Experiment	12.58812904	12.58797073	52.790	68.82	71.41	13.1020	13.102047
8	Tee or Wye	24.51003265	24.51003265	N/A	68.82	68.82	24.9047	24.904732
9	HX-1	37.28645325	26.13249969	52.807	71.42	68.82	38.1745	27.020298
10	Throttle Valve	47.42216492	39.25186920	52.807	71.42	71.42	48.3102	40.139946
11	Shut Off Valve	0.29266548	0.27489281	52.824	71.42	71.42	1.1813	1.163533
15		38.14276505	38.12500381	52.807	71.42	71.42	39.0308	39.013081
17	Tee or Wye	38.48319244	38.48319244	N/A	71.42	71.42	38.8778	38.877769
18	Tee or Wye	38.77157593	38.77157593	N/A	71.42	71.42	39.1662	39.166153
X24	Valve	24.90473175	2.10972023	0.000	71.41	71.41	24.9047	2.109720
26	DU Target	No Solution	No Solution	0.000	No Solution	No Solution	No Solution	No Solution
X27	Valve	No Solution	39.31039429	0.000	No Solution	71.42	No Solution	39.310394
X28	Valve	39.59877396	No Solution	0.000	71.42	No Solution	39.5988	No Solution
38	Deionizer	1.24195576	1.20342541	1.927	71.42	71.42	1.4641	1.425606
41	Particulate Filter	39.11655807	38.56645584	52.807	71.42	71.42	40.0046	39.454533
44	Area Change	-0.02286053	-0.00141048	52.807	71.41	71.41	0.8652	-0.001278
45	Area Change	0.43248558	-0.89626217	52.824	71.42	71.42	0.4326	-0.007622
46	Tee or Wye	-0.00005913	-0.00005913	N/A	71.41	71.41	0.0000	0.000000
47	Assigned Pressure	0.00000000	0.00000000	0.000	65.00	65.00	0.0000	0.000000
49	Tee or Wye	47.81123352	47.81123352	N/A	71.42	71.42	48.4460	48.446022
51	Valve	46.76284790	1.43805695	1.927	71.42	71.42	46.9950	1.660236
52	Valve	38.43114471	38.41338348	52.807	71.42	71.42	39.3192	39.301460
53	Valve	1.00732708	1.00288296	1.927	71.42	71.42	1.2295	1.225063
54	Area Change	15.69000244	14.28828621	52.790	68.82	68.82	16.5778	14.802204
55	Bend	13.32298660	12.68416405	52.790	68.82	68.82	13.8369	13.198082
56	Bend	12.49266815	11.85364723	52.807	71.41	71.41	13.0067	12.367723
57	Area Change	10.89571381	9.49356079	52.807	71.41	71.41	11.4098	10.381636
60	Area Change	-0.06953335	-0.04237747	54.734	71.42	71.42	0.8845	0.884342
62	Tee or Wye	0.39396381	0.39396381	N/A	71.42	71.42	1.0289	1.028913





## **Chemical Sciences and Engineering Division**

Argonne National Laboratory  
9700 South Cass Avenue, Bldg. 205  
Argonne, IL 60439-4837

[www.anl.gov](http://www.anl.gov)



Argonne National Laboratory is a U.S. Department of Energy  
laboratory managed by UChicago Argonne, LLC